NACA

RESEARCH MEMORANDUM

LARGE-SCALE WIND-TUNNEL TESTS OF AN AIRPLANE MODEL

WITH A 45° SWEPTBACK WING OF ASPECT RATIO 2.8

EMPLOYING HIGH-VELOCITY BLOWING OVER THE

LEADING- AND TRAILING-EDGE FLAPS

By David H. Hickey and Kiyoshi Aoyagi

Ames Aeronautical Laboratory
Moffett Field, Calif.

NATIONAL ADVISORY COMMITTEE
FOR AERONAUTICS
WASHINGTON
May 26, 1958

NATIONAL ADVISORY COMMITTEE FOR AERONAUTICS

RESEARCH MEMORANDUM

LARGE-SCALE WIND-TUNNEL TESTS OF AN AIRPLANE MODEL

WITH A 45° SWEPTBACK WING OF ASPECT RATIO 2.8

EMPLOYING HIGH-VELOCITY BLOWING OVER THE

LEADING- AND TRAILING-EDGE FLAPS

By David H. Hickey and Kiyoshi Aoyagi

SUMMARY

An investigation was conducted to determine the longitudinal
characteristics of an airplane model with a thin, highly swept and tapered
wing of low aspect ratio equipped with plain leading-edge flaps in con-
junction with blowing-type boundary-layer control applied to the flap
radius. In these tests blowing-type boundary-layer control was also
applied to a plain trailing-edge flap deflected 60°. Several leading-
edge configurations and boundary-layer control system variables were
investigated.

It was found that leading-edge-blowing boundary-layer control
significantly increased maximum lift and improved stability near maximum
lift. Lift and stability generally were sensitive to spanwise variations
of leading-edge flap deflection and extent of blowing boundary-layer
control.

Blowing momentum coefficient requirements for the leading-edge flaps
were independent of nozzle height and free-stream airspeed. Increasing
angle of attack increased critical momentum coefficient values.

Comparison of the results of this investigation with the results from
another model configuration with the same wing and area-suction boundary-
layer control showed blowing-type boundary-layer control produced larger
lift increments with approximately the same boundary-layer control air
flow.

Estimations of low-speed performance indicate leading-edge boundary-
layer control reduced approach speed 20 percent and take-off ground roll
and distance to 50-foot altitude by about 40 percent. *(for what wing loading and
what installed power?)*

INTRODUCTION

The use of thin, low-aspect-ratio, sweptback wings on modern aircraft seriously limits the low-speed maximum lift and longitudinal stability. A number of studies have been made of the effectiveness of boundary-layer control on wing flaps as a means of improving the low-speed characteristics of such airplanes. Some of the results obtained are presented in references 1 through 6. Results of tests of a 35° swept wing with area suction and blowing applied to the trailing-edge flaps are reported in references 1 and 2, respectively. References 3 and 4 report results of blowing boundary-layer control applied to trailing-edge and leading-edge flaps on a 49° swept wing. A study has also been made on a wing having 45° of sweep, an aspect ratio of 2.8, a taper ratio of 0.17, and a thickness ratio of 0.05. Results of tests with area-suction trailing-edge flaps are presented in reference 5. To control leading-edge air-flow separation, area suction was effectively applied at the radius of the leading-edge flap as reported in reference 6.

The present investigation was conducted to examine the effectiveness of blowing boundary-layer control applied to the hinge-line radius of the leading-edge flap on the latter wing plan form. For this investigation, the emphasis was placed on increasing maximum lift and retaining stability to maximum lift. Longitudinal characteristics were determined for two spanwise extents of trailing-edge flaps, three spanwise extents of leading-edge flap deflection, and various amounts of boundary-layer control. Corresponding leading-edge and trailing-edge boundary-layer control jet-momentum requirements were determined. An estimation of the effect of leading-edge flap boundary-layer control on low-speed performance is included. Results from a two-dimensional investigation conducted in a 2- by 5-foot wind tunnel are included to supplement the three-dimensional leading-edge jet-momentum requirement data.

NOTATION

b   wing span, ft

BLC   boundary-layer control

c   chord, measured parallel to the plane of symmetry, ft

c'   chord, measured normal to the wing leading edge, ft

$\bar{c}$ mean aerodynamic chord, $\dfrac{2}{S}\displaystyle\int_0^{b/2} c^2 dy$, ft

C_D drag coefficient, $\dfrac{\text{drag}}{q_\infty S}$

C_L lift coefficient, $\dfrac{\text{lift}}{q_\infty S}$

ΔC_L increment in lift coefficient due to leading-edge boundary-layer control or trailing-edge flap deflection

ΔC_{LS} increment in lift coefficient for tip stall

C_m pitching-moment coefficient computed about $0.25\bar{c}$, $\dfrac{\text{pitching moment}}{q_\infty S \bar{c}}$

C_Q flow coefficient, $\dfrac{Q}{U_\infty S}$

C_μ momentum coefficient, $\dfrac{W_j/g}{q_\infty S} V_j$

d distance from the engine thrust line to the moment center, ft

D drag, lb

F_G gross thrust from engine, $\dfrac{W_e V_{TP}}{g}$, lb

F_n net thrust from engine, $\dfrac{W_e V_{TP}}{g} - \dfrac{W_e U_\infty}{g}$, lb

g acceleration of gravity, 32.2 ft/sec^2

h nozzle height, inches, or altitude of the airplane, ft

L lift, lb

$L.E.$ leading edge

l distance parallel to the plane of symmetry between the moment center and the effective turning point of the engine air at the inlet, ft

l_t distance from the quarter-chord point of the wing mean aerodynamic chord to the quarter chord of the horizontal-tail mean aerodynamic chord, ft

p   static pressure, lb/sq ft

p_t total pressure, lb/sq ft

q_∞ free-stream dynamic pressure, lb/sq ft

Q   volume flow of boundary-layer-control air under standard conditions, cu ft/sec

R   Reynolds number, $\dfrac{U_\infty \tilde{c}}{\nu}$, or gas constant for air, 53.3 ft-lb/lb-°R

S   wing area without chord extension added, sq ft, or total take-off distance, ft

S_g take-off ground roll, ft

S_t air distance over a 50-foot obstacle, ft

t   time, sec

T_t total temperature, °R

T.E.   trailing edge

U_∞ free-stream velocity, ft/sec

V   velocity, knots

V_j jet velocity assuming isentropic expansion,

$$\sqrt{\frac{2\gamma}{\gamma-1}\, gRT_{t_d}\left[1 - \left(\frac{p_\infty}{p_{t_d}}\right)^{\frac{\gamma-1}{\gamma}}\right]},\ \text{ft/sec}$$

V_{TP} velocity at exit of engine tail pipe, ft/sec

W   gross weight, lb, or weight rate of flow, lb/sec

x   streamwise distance along airfoil chord, ft

y   spanwise distance perpendicular to the plane of symmetry, ft

z   perpendicular distance above the extended wing chord plane, ft

α angle of attack of fuselage reference line, deg

Γ dihedral, deg

δ flap deflection measured normal to the flap hinge line, deg

ν kinematic viscosity of air, ft^2/sec

η pump efficiency, or wing semispan station, $\dfrac{2y}{b}$

γ ratio of specific heats, 1.4 for air, and flight path angle, radians

θ angular distance between flap nozzle and the perpendicular from the flap hinge line to the airfoil chord line (fig. 6), deg

μ rolling friction coefficient

<center>Subscripts</center>

BP   engine bleed port

c   critical

d   flap duct

e   engine

G   on the ground

j   flap jet

le   leading edge

max   maximum

s   stall with power on, or point of initial separation

t   tail

te   trailing edge

to   take-off

u   uncorrected

TP   engine tail pipe

∞ free stream

MODEL AND APPARATUS

Figure 1 is a photograph of the model mounted in the Ames 40- by 80-foot wind tunnel. A drawing of the model is shown in figure 2, and additional geometric data are given in table I.

Wing

Plan form and airfoil section.- The basic wing had a quarter-chord sweep of 45°, aspect ratio of 2.8, and a taper ratio of 0.17. In addition, the basic wing had a 10-percent chord extension, measured parallel to the plane of symmetry, from $\eta = 0.7$ to 1.0. This configuration was used for the entire test program and is called the basic configuration. Airfoil sections parallel to the model plane of symmetry were modified NACA 0005-63 sections, coordinates of which are listed in table II.

Leading-edge flap.- The leading-edge flap was divided into three sections with flap breaks parallel to the plane of symmetry. The flap sections extended from $\eta = 0.15$ to 0.4, 0.4 to 0.7, and 0.7 to 1.0 and will be referred to hereinafter as root, intermediate, and tip leading-edge flap sections, respectively. Listing of the leading-edge flap deflections will follow the same order. For a typical case, $\delta_{le} = 30,60,60$ indicates the root flap section was deflected 30° and the intermediate and tip sections were deflected 60°.

Trailing-edge flap.- Small- and large-span trailing-edge flaps were used during the tests. The small-span flap extended from $\eta = 0.21$ to 0.46 and had a constant 25-percent wing chord, measured parallel to the plane of symmetry. The large-span flap was formed by combining the small-span flap with one which extended from $\eta = 0.46$ to 0.66 and also had a constant 25-percent chord. Both flaps rotated about a hinge near the wing lower surface.

Blowing nozzles.- A typical cross section of the leading-edge flap nozzle is shown in figure 3(a). The nozzle was a slit located on the hinge-line radius of the flap and extended from $\eta = 0.15$ to 1.0. The chordwise nozzle position of 35.5° as shown in figure 3 was maintained throughout the three-dimensional tests. During the investigation, two nozzle heights on the tip leading-edge flap were used. A nozzle height of 0.010 inch on both the intermediate and tip flap sections will be referred to hereinafter as leading-edge flap nozzle A, and a nozzle height of 0.050 inch on the tip section with 0.010 inch on the intermediate section will be referred to as nozzle B.

A trailing-edge flap nozzle cross-section is shown in figure 3(b). The nozzle extended from η = 0.21 to 0.66. A chordwise nozzle position of 22.5° with a nozzle height of 0.020 inch was maintained throughout the investigation.

Leading-edge modifications.- Changes in leading-edge contour as shown in figure 4 were made by increasing the leading-edge radius to approximately 0.9-percent c' and adding a small amount of leading-edge camber. The coordinates for the L.E. modifications are listed in table III. Two spanwise extents of modified leading edge extending from η = 0.4 to 1.0 and 0.7 to 1.0 were tested.

Tail

A swept horizontal tail (fig. 2) was used and was installed with its root at approximately 0.31 of the wing semispan above the extended wing chord plane. The tail was drooped at 20° about a line parallel to the plane of symmetry and the extended wing chord plane. Except where specified, both horizontal and vertical tails were on the model throughout the tests.

Fuselage and Engines

The wing was located approximately 0.13 of the wing semispan below the fuselage center line. The fuselage coordinates are listed in table IV. Compressor bleed from two J-34 turbojet engines, installed side by side inside the fuselage, supplied the blowing boundary-layer control air. The left engine supplied air to the leading-edge flaps; the right engine supplied the trailing-edge flaps. Engine bleed ports were enlarged to allow larger quantities of air to be bled from the compressor.

Boundary-Layer-Control Air Ducting

Ducting to the leading- and trailing-edge flaps is shown in figure 5. The amount of bleed air delivered to the root, intermediate, and tip leading-edge flap sections, and the inboard and outboard portion of the trailing-edge flaps was controlled by butterfly valves in each duct. Total- and static-pressures and temperature measurements to obtain total weight rate of flow to the leading-edge flaps were taken at station 1 in figure 5. For the inboard and outboard portions of the trailing-edge flaps, measurements to obtain weight rate of flow were taken at stations 2

and 3, respectively. Total-pressure and temperature measurements used
for calculating jet-momentum flow were taken at each of the entrances to
the flap ducts (stations 4 through 13 in fig. 5).

Two-Dimensional Airfoil

The airfoil, tested in a 2- by 5-foot wind tunnel, had a 2-foot
chord section and a leading-edge flap hinged at 13.55-percent chord as
shown in figure 6. Coordinates of the airfoil are also given in fig-
ure 6. The flap had a blowing nozzle which could be rotated around the
hinge-line radius of the flap. The airfoil extended across the 2-foot
width of the wind tunnel with pressure orifices located on the upper and
lower surfaces of the airfoil center line.

TESTING AND PROCEDURE

Three-Dimensional Tests

Force and moment data were obtained for the three-dimensional model
through an angle-of-attack range of $0°$ to $33°$. Model configurations for
which force data were obtained are listed in table V which may also be
used as an index to the basic data. All tests, except for the brief
tests at a higher free-stream velocity ($U_\infty = 159$ ft/sec, $R = 11.1 \times 10^6$)
with variable C_μ and the two-dimensional tests, were made at
$U_\infty = 112$ ft/sec corresponding to a Reynolds number of 8.3×10^6. This
Reynolds number corresponded to a free-stream dynamic pressure of
15 pounds per square foot.

Tests at variable angle of attack and constant C_μ.- A major part
of the data was obtained with the plain leading-edge flap with and with-
out blowing and with the trailing-edge flap deflected $60°$ with and with-
out blowing. Various combinations of leading-edge flap deflections, as
shown in table V, were tested. The modified leading edge was tested with
the leading-edge flap deflected with blowing and with the small-span
trailing-edge flap with blowing. Since this report is concerned prima-
rily with the study of the wing leading edge, a constant $C_{\mu_{te}}$ well
above that required for flow attachment on the trailing-edge flap was
maintained when blowing was utilized on the flap.

Tests with variable C_μ at constant angle of attack.- Momentum
coefficient was varied on the intermediate and tip leading-edge flap sec-
tions either together or independently to determine its effect on the
longitudinal characteristics of the model with the following variables:
(1) free-stream velocity, and (2) nozzle heights of 0.010 and 0.050 inch

on the tip flap section. For the small- and large-span trailing-edge flaps, $C_{\mu_{te}}$ was varied at several angles of attack with the flap deflected 60°.

Two-Dimensional Tests

Two-dimensional tests in the 2- by 5-foot wind tunnel were used to investigate the effect of the chordwise location of an $h/c = 0.00033$ leading-edge nozzle on flow requirements. The nozzle location was varied from 6° to 66° with respect to the reference line (fig. 6) and with the flap deflected 60°. Tests were conducted at $\alpha = 36°$ with a free-stream dynamic pressure of 20 pounds per square foot, corresponding to a Reynolds number of 1.6×10^6 based on a 2-foot chord.

Measurement of Engine Thrust

The gross thrust of the engine (for a given configuration a function of $p_{t_{TP}}/p_\infty$) used for thrust corrections to the force data was obtained by calibration of the tail-pipe total-pressure measurement instrumentation with the wind-tunnel balance system. Engine weight rate of flow was obtained from the total-pressure and temperature measurements of the tail-pipe nozzles by means of the following equation:

$$W_e = \frac{F_G g}{V_{TP}}$$

CORRECTIONS TO DATA

Effects of Wind-Tunnel Walls

The following corrections for the effects of wind-tunnel-wall interference were made:

$$\alpha = \alpha_u + 0.75\ C_L$$

$$C_D = C_{D_u} + 0.013\ C_L^2$$

$$C_m = C_{m_u} + 0.005\ C_L$$

Effects of Engine Operation

Force data from the wind-tunnel balance system were corrected for
the effects of engine thrust as follows:

$$C_L = \frac{\text{total lift}}{q_\infty S} - \frac{F_G \sin \alpha}{q_\infty S}$$

$$C_D = \frac{\text{total drag}}{q_\infty S} + \left(\frac{F_G}{q_\infty S} \cos \alpha - \frac{W_e U_\infty}{g q_\infty S} \right)$$

$$C_m = \frac{\text{total moment}}{q_\infty S \bar{c}} + \left[\frac{F_G}{q_\infty S} \frac{d}{\bar{c}} - \frac{W_e U_\infty}{g q_\infty S \bar{c}} \left(l \sin \alpha + d \cos \alpha \right) \right]$$

These corrections include the force due to turning the engine air at the
inlets when the airplane model is at an angle of attack.

RESULTS

Configurations for which the force data are presented herein are
listed in table V. Three-component force data showing the longitudinal
characteristics of the model with the small-span flap are presented in
figures 7 through 10. Figure 7 presents a summary of the effect of
leading-edge flap deflection and BLC on the longitudinal characteristics
of the model. More detailed data are presented in figure 8. Figure 9
presents results showing the effects of spanwise extent of blowing
boundary-layer control, and figure 10, the effects of the modified lead-
ing edge. Results for two spanwise extents of trailing-edge flap are
shown in figure 11.

Data showing the influence of jet momentum on lift are presented in
figures 12 through 17. Results included are the effects on leading-edge
BLC requirements of nozzle height, free-stream velocity, angle of attack,
and blowing nozzle position on the leading-edge flap radius. Trailing-
edge flap C_μ requirements are also shown.

Figures 18 and 19 compare results of this investigation (blowing
BLC) and of reference 6 (area-suction BLC) to facilitate comparison of
the two types of BLC with respect to longitudinal characteristics and
ΔC_{L_S}, the delay in tip stall, due to leading-edge flap deflections.

Results of calculations to show the effect of leading-edge blowing
BLC on landing approach speed are shown in figure 20. Figures 21, 22,

and 23 present the calculations that show the effect of leading-edge BLC on take-off ground roll distance, air distance to 50-foot altitude, and total distance to 50-foot altitude.

Results of design calculations to determine the leading-edge BLC system characteristics used in the performance analysis are presented in figures 24 through 26.

DISCUSSION

This investigation was directed at increasing maximum lift while retaining longitudinal stability. The data in figure 7 show that, for the wing plan form considered here, trailing-edge flaps with BLC reduced the angle of attack for a given lift coefficient below maximum lift, but did not significantly increase maximum lift. In view of this, the major portion of the discussion will consider the effects on maximum lift and longitudinal stability of a plain leading-edge flap with blowing BLC applied on the flap radius.

The term "usable lift coefficient," as employed in the following discussion, is defined as the lift coefficient at which neutral longitudinal stability occurs; increasing lift above this value causes longitudinal instability.

Summary of the Effect of the Leading-Edge Flap and Leading-Edge BLC on Longitudinal Characteristics

Data presented in figure 7 show the maximum gains realized in the tests. Deflection of only the trailing-edge flaps with BLC gave little increase in maximum lift coefficient or usable C_L. The deflection of the leading-edge flaps without leading-edge BLC increased $C_{L_{max}}$ from 0.99 to 1.25, but usable C_L was increased only from 0.83 to 1.0. Application of leading-edge BLC with larger leading-edge flap deflections increased $C_{L_{max}}$ to 1.61 and usable C_L to 1.59. The combination of leading-edge flap deflection and blowing leading-edge BLC increased usable C_L 91 percent. A large portion of this gain was the result of leading-edge BLC extending the range of longitudinal stability so that usable C_L was near $C_{L_{max}}$.

Effect of Leading-Edge Configuration Variables
on Longitudinal Characteristics

For this wing plan form, air-flow separation occurred first at the wing leading edge at the outboard wing sections and then progressed inboard with increased angle of attack. This stall progression resulted in longitudinal instability. In order to increase maximum lift and also retain longitudinal stability with BLC, it was necessary to have larger leading-edge flap deflections outboard than inboard and also to control the spanwise amount of BLC.

Effect of leading-edge flap deflection.- Data showing the effect of several combinations of leading-edge flap deflection on lift and stability are presented in figure 8. These data include results without leading-edge BLC, and with leading-edge BLC for the two leading-edge nozzles tested. The lift results are summarized as follows:

δ_{le}, deg	Leading-edge nozzle	$C_{\mu_{le}}$	$C_{L_{max}}$	$\Delta C_{L_{max}}$	Usable C_L	Usable ΔC_L
0,0,0	- -	0	0.99	(a)	0.83	---
0,40,50	- -	0	1.25	0.26	1.00	0.17
0,50,60	- -	0	1.22	.23	1.00	.17
0,60,60	- -	0	1.20	.21	1.00	.17
30,60,60	- -	0	1.06	.07	.98	.15
0,40,50	A	.027	1.32	b.07	1.26	.26
0,50,60	A	.027	1.40	.15	1.28	.28
0,60,60	A	.027	1.44	.19	1.40	.40
c30,60,60	B	.030	1.51	.26	1.50	.52
0,40,50	B	.076	1.40	b.15	1.32	.32
0,50,60	B	.076	1.45	.20	1.44	.44
0,60,60	B	.076	1.48	.23	1.48	.48
30,60,60	B	.076	1.61	.36	1.59	.59

[a]Increments from $\delta_{le} = 0,0,0$ values
[b]Increments from $\delta_{le} = 0,40,50$ values with $C_{\mu_{le}} = 0$
[c]From figure 9(c)

The optimum leading-edge flap deflection without BLC ($\delta_{le} = 0,40,50$) increased $C_{L_{max}}$ by 26 percent and usable C_L by 20 percent. With $C_{\mu_{le}} = 0.027$ and the leading-edge flap deflection increased to $60°$ at the intermediate and outboard sections, $C_{L_{max}}$ was increased by 45 percent and usable C_L by 69 percent. With a larger $C_{\mu_{le}}$ (0.076), these values were 49 and 78 percent, respectively. Strong nose-down moments

beyond $C_{L_{max}}$ and the relatively small increase in $C_{L_{max}}$ when $C_{\mu_{le}}$ was increased indicated that the maximum lift of this configuration was limited by air-flow separation over the root section.

Protection against the root stall was provided by 30° of leading-edge flap deflection without BLC. This amount of root protection in conjunction with the intermediate and tip sections deflected 60° with BLC ($C_{\mu_{le}}$ = 0.030) increased $C_{L_{max}}$ by 53 percent and usable C_L by 81 percent. Corresponding increases with $C_{\mu_{le}}$ = 0.076 were 63 and 91 percent, respectively. Increasing root protection by increasing the root flap deflection to 50° and applying BLC increased $C_{L_{max}}$ only an additional 3 percent (see fig. 8(d)). This small gain indicates that if a further gain in $C_{L_{max}}$ is to be realized, more effective flow control is required at the intermediate and tip sections. Increasing leading-edge flap deflection or $C_{\mu_{le}}$ can provide the additional control.

<u>Effect of spanwise distribution of blowing BLC.</u>- Limitations on the quantity of available bleed air or duct size may require some variations in the spanwise extent and quantity of blowing BLC. Figure 9 presents data showing the effects of such variations on the longitudinal characteristics of the model. The effect of blowing over the tip section alone compared with blowing over the tip and intermediate sections is shown in figure 9(a) and the pertinent data are tabulated below for δ_{le} = 0,50,60.

C_μ		$C_{L_{max}}$	Usable C_L
η = 0.4 to 0.7	η = 0.7 to 1.0		
0	0	1.22	1.00
0	.011	1.24	1.12
.013	.014	1.40	1.30
0	.057	1.30	1.22
.014	.060	1.45	1.45

The importance of blowing on the intermediate section in conjunction with blowing on the tip is apparent since increments of usable C_L of 0.18 and 0.23 were gained.

The effect of blowing increased amounts of BLC air over the tip section with a constant amount of blowing over the intermediate section is shown in figure 9(b). No appreciable gain in usable C_L was obtained. However, it is believed that with a 30° root-flap deflection rather than the 0° flap tested, an appreciable gain in C_L would have been realized. This assertion is partially substantiated by data presented later

(fig. 14(b)) showing the variation of C_L with $C_{\mu_{le}}$ at $\alpha = 25.2^\circ$ and $\delta_{le} = 30,60,60$. The same increase in tip section blowing as that for the data in figure 9(b) with $\delta_{le} = 30,60,60$ increased C_L by 0.12.

The effect on C_{Lmax} and usable C_L of varying $C_{\mu_{le}}$ from 0.030 to 0.078 (see fig. 9(c)) was small ($\Delta C_{Lmax} = 0.1$) when compared with the gain obtained by increasing $C_{\mu_{le}}$ from 0 (fig. 8(a)) to 0.030. These data had a tip to intermediate section blowing ratio of between 5 and 7 to 1 and the root flap deflected 30°. Data in a later section of this report show that the lowest $C_{\mu_{le}}$ tested from $\eta = 0.4$ to 1.0 (0.030) was adequate to provide BLC over the leading-edge flap radius as long as unseparated air flow existed in front of the leading-edge nozzle. Further reduction of $C_{\mu_{le}}$ (keeping the same spanwise flow distribution) would have allowed flow separation on the flap radius at the intermediate section and, perhaps, a resultant deterioration of longitudinal characteristics.

Effect of increased leading-edge radius and camber.- Research on increasing C_{Lmax} by enlarging the leading-edge radius and cambering the forward portion of the airfoil is reported in reference 7. Reference 5 presents results of tests on this modification in conjunction with a plain leading-edge flap, and reference 6 extends these data to the case with area suction applied to the radius of the flap. All three of these references report that the leading-edge modification improved longitudinal characteristics.

Details of this modification as applied in the present test are shown in figure 4. The effect on the longitudinal characteristics of applying this modification on two spanwise extents of the leading edge is shown in figure 10. No appreciable gain in C_{Lmax} or usable C_L resulted from the application of the modification to the tip section. With the modification on both the intermediate and tip flap sections, C_{Lmax} and usable C_L were increased 0.05, and the angle of attack for C_{Lmax} was increased 1°. This gain is smaller than would be anticipated from the data in references 5, 6, and 7.

<center>Trailing-Edge Flaps</center>

The data in figure 7 show that without leading-edge BLC, the small-span trailing-edge flap with area-suction BLC had little effect on C_{Lmax} or usable C_L, but served mainly as a device to reduce the angle of attack for a given C_L below C_{Lmax}.

Longitudinal characteristics.- Although trailing-edge flap blowing BLC did increase C_{Lmax} and usable C_L when accompanied by leading-edge BLC (fig. 11), the magnitude of the gains was small relative to the increases provided by leading-edge flap BLC. With BLC applied to

the small-span trailing-edge flaps, usable C_L and $C_{L_{max}}$ were increased by values of 0.09 and 0.07, respectively, whereas both increments of gain were 0.16 with BLC applied to the large-span flaps.

A reflex in the lift curve occurred when leading-edge BLC was applied without BLC on the trailing-edge flap. Static-pressure orifices near the trailing-edge flap radius showed that the minimum pressure on the flap approached the values obtained with trailing-edge BLC applied as the angle of attack was increased to about 8°. An apparent increase in lift-curve slope resulted which reduced the angle-of-attack changes due to trailing-edge BLC for a given C_L. In the α range consistent with the landing approach condition ($\alpha = 12^\circ$ to 16°), trailing-edge BLC reduced the angle of attack for a given C_L by about 1-1/2° for the small-span flap and 4-1/2° for the large-span flap.

Comparison with theory.- The theoretical lift increment obtainable from the deflected trailing-edge flaps used in this investigation was calculated by the method of reference 8. These increments for $\delta_{te} = 60^\circ$ are shown below.

Flap span, η	Experimental ΔC_L (tail on)	Theoretical ΔC_L
0.21 - 0.46	0.43	0.53
.21 - .66	.77	.86

The experimental results listed above were obtained by extrapolation to $\alpha = 0^\circ$ of the data in figure 11. The decrement of ΔC_L due to the tail is estimated to be 0.05 for the small-span trailing-edge flap and 0.08 for the large-span trailing-edge flap.

Boundary-Layer-Control Flow Requirements

It was found in reference 2 that the C_{μ_c} required for a given trailing-edge configuration was dependent on flap deflection and nozzle location, and was independent of nozzle height, free-stream airspeed, and angle of attack. In the case of the leading-edge flap, the minimum pressure and pressure gradient on the leading-edge flap radius is dependent to some degree on angle of attack, so that leading-edge BLC flow requirements should also be dependent on angle of attack.

Figure 12 contains data showing the variation of C_L with $C_{\mu_{le}}$ for two blowing nozzle heights, two free-stream airspeeds, and two angles

of attack. These data indicate that, within the limits tested, lift
obtained from $C_{\mu_{le}}$ is independent of nozzle height and free-stream
airspeed, and is dependent upon angle of attack.

Variation of leading-edge BLC flow requirements with angle of
attack.- Figures 13 and 14 present data showing the variation of C_L
with $C_{\mu_{le}}$ for several angles of attack. Figure 15 presents a cross
plot of the data in figures 13 and 14, showing the variation of critical
$C_{\mu_{le}}$ with C_L. Critical $C_{\mu_{le}}$ for the data in figure 15 was arbitrarily
defined as the point where the slope of C_L versus $C_{\mu_{le}}$ curve equals 8,
and approximately corresponds to the point where BLC at the flap radius
is realized without air-flow separation in front of the blowing nozzle.

These data show a rapid increase in total C_{μ_c} with lift coefficient
(or α). In general, the tip wing section had a larger value of C_{μ_c}
than the intermediate section. This was due to the high section lift
coefficients (when compared to the intermediate section) on the tip sec-
tion of a wing with this plan form. Further, pressure distributions
indicated that at $\alpha = 25.2^\circ$, some flow separation existed in front of
the BLC nozzle. The blowing BLC caused the flow to reattach, but at
relatively high $C_{\mu_{le}}$ values. This could explain the rapid increase in
C_{μ_c} above $C_L = 1.35$ for intermediate and tip blowing shown in figure 15.

Delaying the stall to a larger angle of attack would require
prevention of the air-flow separation in front of the leading-edge blow-
ing nozzle by larger flap deflections or BLC on the flap leading edge.
The other alternative is provision for extremely large $C_{\mu_{le}}$ values on
the flap radius to induce flow reattachment.

Effect of leading-edge-blowing nozzle position.- Reference 2 reported
that C_μ requirements were independent of nozzle position on the
trailing-edge flap radius as long as the nozzle was upstream from the
minimum pressure point. A downstream position of the nozzle was found
to increase the flow requirements.

The leading-edge nozzle was placed at $\theta = 35.5^\circ$ during the three-
dimensional model investigation. The angle θ is shown in figure 6.
This location was selected on the basis of results from an exploratory
two-dimensional investigation. These data are presented in figure 16.
The trend exhibited by the two-dimensional results is similar to those
observed in reference 2. Placement of the nozzle downstream of the min-
imum pressure ($\theta = 36^\circ$) greatly increased the BLC flow requirements;
however, placement upstream caused no noticeable change. For all flap
deflections tested during the three-dimensional model investigation,
the leading-edge BLC nozzle was at or upstream from the point of minimum
pressure on the flap radius.

Trailing-edge flap flow requirements.- Figure 17 presents data
showing the variation of C_L with $C_{\mu_{te}}$. The data for the two trailing-
edge flaps were obtained with different leading-edge flap configurations.
The data indicate that C_{μ_c} = 0.0015 and 0.006 with δ_{te} = 60° for the
small-span and large-span flaps, respectively. It is believed that at
α = 0° these values were unaffected by the different leading-edge
configurations.

Reference 2 gives a relationship for determining the equivalent
two-dimensional C_μ from three-dimensional data. The data from the
present investigation were used to obtain equivalent two-dimensional
values of 0.0075 and 0.019 for the small- and large-span flaps, respec-
tively. These are only 22 percent and 56 percent of the value (0.034)
quoted in reference 2 for δ_{te} = 60°.

Comparison of Blowing and Area-Suction Boundary-
Layer Control

Since both area-suction (ref. 6) and blowing boundary-layer control
investigations have been conducted on the same wing, some comparison of
the effectiveness of the two types of BLC should be made. Although the
wing and horizontal tail of the two models were actually the same for
both investigations, the fuselages, wing height, and tail height were
somewhat different. The over-all effect of these differences on the
basic model without boundary-layer control was that the maximum lift
coefficient and the lift-curve slope were less for the low-wing model
than for the mid-wing model, as shown in figure 18. Also shown in the
figure is the comparison with blowing and suction, indicating that blow-
ing was more effective than suction in increasing maximum lift as well
as retaining linear lift and pitching-moment characteristics to higher
values of lift coefficient. In support of the foregoing, figure 19 has
been prepared to show the relative effectiveness of the two types of BLC
in preventing outboard stall as indicated by changes in drag and pitch-
ing moment and limited observations of pressure distributions. Identical
spanwise configurations of leading-edge flap deflections were not tested;
however, the results shown for the outboard flap should indicate the
effectiveness of each system in preventing outboard stall. The value of
ΔC_{L_S} shown in the figure corresponds to the increment of lift by which
air-flow separation on the outboard sections is delayed from the value of
lift coefficient at which separation occurred with no leading-edge flap
deflections. Blowing provides significantly greater values of ΔC_{L_S}
than area suction through the range of outboard flap deflections tested.

To illustrate the relative engine bleed-air requirements of the
two boundary-layer-control systems a comparison has been made for condi-
tions where each system achieved about the same lift coefficient
(C_L of about 1.4) at an angle of attack of 21° or 22°. For this

comparison suction BLC was given the added advantage of a modified
leading edge. With area suction, reference 6 shows that a flow coeffi-
cient of about 0.001 is required, whereas for blowing the present inves-
tigation shows a momentum coefficient, C_μ, of about 0.020 is required.
The engine bleed-air requirements for each system were calculated by the
method discussed in reference 2, assuming a flight speed of 130 knots
and bleed air available from the engine at a pressure ratio of 5.0 and
at a temperature of 900° R. The engine bleed air was used directly for
blowing BLC, whereas it was used to drive a pump for area-suction BLC.
With a pump of 80-percent efficiency the area-suction system would
require about 30 percent of the bleed air required for blowing; with a
pump of 15-percent efficiency (an ejector pump), the area-suction system
would require about 140 percent of that for blowing.

It can be concluded as was the case for trailing-edge flaps (ref. 2)
that blowing systems will require the same order of bleed air from the
engine as area suction unless the latter use reasonably efficient pumping
systems.

Evaluation of Blowing Boundary-Layer Control

Pertinent low-speed performance with and without blowing boundary-
layer control is considered here. Results of computations of approach
speed and take-off distance are presented. Details of the blowing noz-
zle size selection and performance calculations are contained in
Appendixes A and B.

Approach speed.- Reference 9 shows 1.15 V_S to be one criterion for
landing-approach speed. This value will be used here. Figure 20(a)
shows approach speed for the best configuration with leading-edge boundary-
layer control (δ_{le} = 30,60,60) and without leading-edge boundary-layer
control (δ_{le} = 0,40,50) with the small-span trailing-edge flap. The
increase in usable C_L obtained with leading-edge boundary-layer control
reduced approach speed at W/S = 55 pounds per square foot by 31 knots
or about 21 percent. The effect of trailing-edge boundary-layer control
with δ_{le} = 30,60,60 and leading-edge BLC (fig. 20(b)) was a 4-knot reduc-
tion of approach speed with the small-span flap. Approach speed was
reduced an additional 5 knots with the large-span flap and BLC. Attitude
of the aircraft during the landing approach was 15° for the small-span
trailing-edge flap with and without BLC, and 12° for the large-span flap
with BLC.

Take-off distance.- The method used and the assumption made in
calculating take-off distance over a 50-foot obstacle are discussed in
Appendix B. Two cases have been analyzed: (1) a minimum lift-off
velocity of 1.05 V_S (angle of attack about 20°), and (2) the velocity
corresponding to lift-off at an angle of attack of 15°.

The reduction in ground-roll distance for take-off with the application of leading-edge flap boundary-layer control is shown in figure 21. For the case of 1.05 V_S, the reduction in ground-roll distance is 37 percent over the entire wing loading range and for the case of a limiting angle of attack of 15° the reduction varies from about 18 percent at a W/S of 70 lb/sq ft to about 22 percent at a W/S of 100 lb/sq ft. For both cases, maximum thrust loss from full engine air bleed with the leading-edge nozzle designed for $C_{L_{max}}$ near $\alpha = 25°$ was used in the calculations. Control of the engine air for the leading-edge BLC system during the take-off (discussed in Appendix A), and the resultant minimization of thrust loss due to BLC caused a further reduction of 150 to 300 feet in ground-roll distance throughout the wing loading range studied.

The reductions in air distance to obtain an altitude of 50 feet with the application of leading-edge BLC are shown in figure 22. Reductions of comparable percentages as in the ground roll are indicated for the low wing loading range of the airplane. However, at wing loadings greater than 80 lb/sq ft, the F_n/W ratio of the airplane without BLC is sufficiently low to leave little or no excess thrust for acceleration; under these conditions, larger reductions in transition distance resulted from the use of BLC, primarily as a consequence of the large reductions in drag. The control of bleed air also shows a more significant reduction in air distance to 50 feet at wing loadings greater than 80 lb/sq ft.

The same trends in reduction in take-off distance with boundary-layer control are shown in figure 23 as the total distance to 50 feet of altitude. To summarize, it appears that the total take-off distance can be reduced by about 38 percent between W/S of 65 to 85 lb/sq ft with reductions greater than 50 percent at W/S about 90 lb/sq ft for take-off based on 1.05 V_S. With the take-off speed limited to an angle of attack of 15°, the reduction in take-off distance varies from a value of about 20 percent at a W/S of 65 to a value of about 30 percent at a W/S of 85 lb/sq ft to greater than 40 percent at higher wing loadings. The use of controlled bleed indicates the largest improvements are to be made at the higher wing loadings corresponding to the lower thrust-to-weight ratios and can result in additional improvements of 1000 to 3000 feet. The thrust-to-weight ratio of the hypothetical airplane was 0.3 at a W/S of 103 lb/sq ft. It therefore appears that controlled bleed during the take-off may provide significant improvement in take-off performance, particularly for airplanes having thrust-to-weight ratios of less than about 0.3

CONCLUSIONS

The following conclusions have been made from analysis of the test results:

1. Leading-edge-blowing boundary-layer control (BLC) significantly increased maximum lift and stability near maximum lift. Lift and stability were generally sensitive to spanwise variations in flap deflection and extent of blowing.

2. Variation of lift with momentum coefficient was independent of blowing nozzle height and free-stream airspeed. Increasing angle of attack increased critical leading-edge momentum coefficient values.

3. The trailing-edge flaps caused a relatively small gain in maximum and usable lift when compared to the leading-edge flaps.

4. Comparison of the results of this investigation with the results of NACA RM A57H21 (area-suction BLC) showed that the increments of maximum and usable lift due to leading-edge BLC were higher with the blowing BLC model. Leading-edge BLC air-flow requirements were of the same order of magnitude for the two types of BLC. Engine bleed-air requirements for the two types of BLC are, however, a function of the particular installation.

5. A limited two-dimensional investigation indicated that location of the blowing nozzle downstream from the point of minimum pressure on the leading-edge·flap radius increased the critical momentum coefficient.

6. Estimation of the low-speed performance improvement obtainable with leading-edge BLC and small-span flap with BLC indicated a reduction in approach speed of 20 percent (based on 1.15 of the stalling speed) and a reduction of take-off distance over a 50-foot obstacle of as much as 40 percent at the higher wing loadings.

Ames Aeronautical Laboratory
        National Advisory Committee for Aeronautics
            Moffett Field, Calif., Jan. 9, 1958

APPENDIX A

DETERMINATION OF THE BOUNDARY-LAYER-CONTROL

SYSTEM CHARACTERISTICS

In evaluating the low-speed performance of an airplane with BLC the following elements in the design of the blowing BLC system were considered from the standpoint of their effects on performance.

Aircraft Size and Power

The wing plan form considered was intended to represent one approach to the wing design of a high-performance fighter aircraft. Data for present-day aircraft indicate that a minimum F_n/W ratio of 0.4 and operation at wing loadings from 50 to 100 lb/sq ft are representative. In accordance with these values, the linear model dimensions were increased 25 percent and two J-57 engines were assumed to be the power plants.

Blowing Nozzle Height Selection

Reference 2 presents a method of matching the requirement of a trailing-edge flap blowing BLC system with the bleed capabilities of a turbojet engine. This method was used for the leading-edge BLC system. The value of $C_{\mu_{le}} = 0.032$ was selected on the basis of the discussion in the present report regarding critical C_μ.

The variation of W_{BP} with duct pressure ratio for constant free-stream velocities was calculated for this C_μ and is shown in figure 24. For the calculations, duct air pressure and temperature were assumed to be the same as at the engine bleed port. Air characteristics at the engine bleed port were obtained from reference 10. Flow conditions through the BLC nozzle were assumed to be isentropic. The variation of W_{BP} with duct pressure ratio for several values of nozzle height were plotted as shown in figure 24.

Based on a design trim $C_{L_{max}}$ of 1.47, wing loadings were assigned to the constant velocity curves. The working area of the chart (fig. 24) is defined by the wing-loading range and pressure ratio available during take-off and landing approach. The large difference in duct pressure ratio available at take-off (10.5) and landing approach (6.2 for 10 ft/sec sinking speed) indicates that the selection of nozzle height is a compromise. The 0.010-inch nozzle height would limit landing approach speed.

The 0.015-inch nozzle used in the calculations is the smallest size that would supply the stipulated C_μ during landing approach; however, this nozzle would pass greater values of bleed air than necessary during take-off if no bleed control is considered. The thrust loss due to air bleed will be discussed in the next section.

The trailing-edge flap nozzle heights selected by the same procedure were very small. From a practical construction standpoint, nozzle heights of 0.010 and 0.015 inch were selected for the small- and large-span flap, respectively.

Reduction of Thrust Losses Due to Boundary-Layer-
Control Air Bleed

Figure 25(a) shows the variation of $C_{\mu_{c_{le}}}$ with angle of attack obtained from figure 15(b). As shown by the figure, $C_{\mu_{c_{le}}}$ increases rapidly with increasing angle of attack. If the nozzle height selection is based on $C_{\mu_{c_{le}}}$ at a high angle of attack, which was the case for the performance estimation here, the engine bleed air for leading-edge BLC would be greatly in excess of that required through most of the take-off and landing-approach maneuver. Examination of the nozzle height chart (fig. 24) shows that at the take-off wing loadings of 90 to 100 lb/sq ft, the hypothetical airplane would have a stalling speed of approximately 140 knots. Figure 25(b) shows the calculated BLC bleed air required at 140 knots with the 0.015-inch leading-edge nozzle as a function of angle of attack. The bleed air supplied by the unrestricted ducting is also shown in the figure. Figure 25(c) shows that, during the take-off ground run, as much as 11.5 percent of the thrust at take-off can be lost due to unrestricted leading-edge BLC bleed air. Restricting the leading-edge BLC engine bleed air during the take-off to required values throughout the range of angles of attack resulted in no thrust loss during ground run to small values during transition. A throttle valve placed in the leading-edge ducting can be used to restrict the BLC engine bleed air flow. This valve could be controlled by a device which senses changes in angle of attack, dynamic pressure, etc.

It is also necessary to check the effect of the bleed air control during the landing approach. Figure 26 presents the variation of C_μ required and available with velocity for 10 ft/sec sinking speed. The thrust component of the lift was ignored for these calculations. For this hypothetical airplane, the bleed air control, designed for the take-off conditions of figure 25, would not supply the $C_{\mu_{le}}$ required during the landing approach. To do this the throttling of the valve must be reduced slightly.

APPENDIX B

PERFORMANCE COMPUTATIONS

The test results used for the low-speed-performance computation were modified as follows:

1. A drag coefficient increment of 0.06 was added to the test values to account for landing gear and airplane protuberances not found on the model.

2. The pitching moment used to obtain the trimmed C_L was taken with the aircraft moment center at $0.33\bar{c}$ instead of $0.25\bar{c}$ as the data are presented.

In addition, the term $C_{L_{max}}$ as used here is synonymous with the term "usable C_L" in the body of the report.

Approach Speed

An evaluation of approach speed for several present-day fighters was made in reference 9, which indicates that a value of $1.15\ V_S$ is one criterion for approach speed and is used herein. For flight at a constant wing loading and rate of sinking speed, the value of V_S is dependent on C_μ available and the corresponding value of $C_{L_{max}}$ obtained. These variables can be obtained from the test results, the BLC system characteristics (as determined in Appendix A), and the engine characteristics during the landing approach. The stall speed was then determined by the following relation for dynamic pressure:

$$q_S = \frac{W/S}{C_L + C_D \tan \alpha}$$

where $C_D \tan \alpha$ is the ΔC_L due to the thrust component in the vertical direction.

Take-Off Distance

In the calculations the maneuver was considered in two parts: the ground roll, and the air distance required to clear a 50-foot obstacle. Ground distance is the distance required for the airplane to accelerate to a predetermined lift-off velocity at $\alpha = 0°$. The airplane is then

rotated to a suitable α for the lift-off with the landing gear down and
held at this angle of attack until the 50-foot height has been reached.
The distance required for this climb is the air distance. A maximum per-
formance take-off dictates that the lift-off should occur at 1.05 V_S
(0.907 $C_{L_{max}}$) and the climb at the angle of attack required for flight
at 1.05 V_S. Since this angle is high (about 20°) with leading-edge BLC,
and ground attitude on an actual aircraft may be limited, take-off dis-
tances with both 1.05 V_S and $\alpha = 15°$ as the criterion are presented.

Data available are insufficient to determine the optimum trailing-
edge configuration for take-off; accordingly, the effects of trailing-
edge configuration on take-off distance will not be considered here.
All calculated take-off distance results are with the small-span flap
deflected 60° with BLC. An NACA standard day is assumed.

The ground roll distance was calculated by the following equation
(from ref. 11):

$$S_g = \frac{13.1 \frac{W}{S}}{C_{L_G}\left(\frac{D}{L} - \mu\right)} \; \ln\left[\frac{\frac{F_n}{W} - \mu}{\frac{F_n}{W} - \mu - \frac{C_{L_G}}{C_{L_{to}}}\left(\frac{D}{L} - \mu\right)}\right]$$

The air distance was obtained by a point-by-point solution of the
equations for the forces on the airplane. These equations are as follows:

$$\frac{dU}{dt} = g\left(\frac{F_n}{W}\cos\alpha - \frac{C_D q S}{W} - \sin\theta\right)$$

$$\frac{d\gamma}{dt} = \frac{g}{U}\left(\frac{C_L q S}{W} + \frac{F_n}{W}\sin\alpha - \cos\theta\right)$$

where γ is the flight-path angle in radians. The finite increments
of U and γ were calculated at 1-second intervals, and the ground distance
and altitude were then obtained by:

$$S_t = \sum_{h=0}^{h=50} (U+\Delta U)\cos\gamma$$

$$h = \sum \gamma(U+\Delta U) \quad \text{(for small values of } \gamma\text{)}$$

For the higher wing loadings, acceleration became zero prior to 50 feet and hence the transition reached completion before an altitude of 50 feet. In these cases, the distance to climb to 50 feet altitude at the steady rate of climb was added to the distance required to complete the transition.

For the purpose of the calculation, the following assumptions and simplifications were made: (1) average thrust was assumed through the speed range, (2) effects of ground proximity were neglected, and (3) the ground-resistance coefficient was $\mu = 0.03$. The effect of thrust loss due to bleed air for BLC was evaluated and hence determined the value of F_n/W. With controlled bleed air, thrust loss due to engine bleed for leading-edge BLC was zero throughout the ground roll, and the minimum during transition, so that the gains realized from controlled bleed were a direct result of increased F_n/W.

REFERENCES

1. Cook, Woodrow L., Hölzhauser, Curt A., and Kelly, Mark W.: The Use
    of Area Suction for the Purpose of Improving Trailing-Edge Flap
    Effectiveness on a 35° Sweptback Wing. NACA RM A53E06, 1953.

2. Kelly, Mark W., and Tolhurst, William H., Jr.: Full-Scale Wind-
    Tunnel Tests of a 35° Sweptback Wing Airplane With High-Velocity
    Blowing Over the Trailing-Edge Flaps. NACA RM A55I09, 1955.

3. Fink, Marvin P., and McLemore, H. Clyde: High-Pressure Blowing Over
    Flap and Wing Leading Edge of a Thin Large-Scale 49° Swept Wing-
    Body-Tail Configuration in Combination With a Drooped Nose and a
    Nose With a Radius Increase. NACA RM L57D23, 1957.

4. McLemore, H. Clyde, and Fink, Marvin P.: Blowing Over the Flaps and
    Wing Leading Edge of a Thin 49° Swept Wing-Body-Tail Configuration
    in Combination With Leading-Edge Devices. NACA RM L56E16, 1956.

5. Koenig, David G., and Aoyagi, Kiyoshi: Large-Scale Wind-Tunnel
    Tests of an Airplane Model With a 45° Sweptback Wing of Aspect
    Ratio 2.8 With Area Suction Applied to Trailing-Edge Flaps and
    With Several Wing Leading-Edge Modifications. NACA RM A56H08,
    1956.

6. Koenig, David G., and Aoyagi, Kiyoshi: The Use of a Leading-Edge
    Area-Suction Flap and Leading-Edge Modifications to Improve the
    High-Lift Characteristics of an Airplane Model With a Wing of 45°
    Sweep and Aspect Ratio 2.8. NACA RM A57H21, 1957.

7. Evans, William T.: Leading-Edge Contours for Thin Swept Wings: An
    Analysis of Low- and High-Speed Data. NACA RM A57B11, 1957.

8. DeYoung, John: Theoretical Symmetric Span Loading Due to Flap
    Deflection for Wings of Arbitrary Plan Form at Subsonic Speeds.
    NACA Rep. 1071, 1952. (Supersedes NACA TN 2278)

9. White, Maurice D., Schlaff, Bernard A., and Drinkwater, Fred J., III:
    A Comparison of Flight-Measured Carrier-Approach Speeds With Values
    Predicted by Several Different Criteria for 41 Fighter-Type Airplane
    Configurations. NACA RM A57L11, 1958.

10. Pratt & Whitney Engine Handbook for J-57-P-1. Specification No.
    A-1632-C, 25 Aug. 1953.

11. James, Harry A., and Maki, Ralph L.: Wind-Tunnel Tests of the Static
    Longitudinal Characteristics at Low Speed of a Swept-Wing Airplane
    With Blowing Flaps and Leading-Edge Slats. NACA RM A57D11, 1957.

TABLE I.- GEOMETRIC DATA

```
Wing
  Area, sq ft (without chord extension) . . . . . . . . . . . . . .   334.8
  Span, ft  . . . . . . . . . . . . . . . . . . . . . . . . . . .    30.62
  Mean aerodynamic chord, ft  . . . . . . . . . . . . . . . . . .    12.77
  Root chord, ft  . . . . . . . . . . . . . . . . . . . . . . . .    18.69
  Aspect ratio  . . . . . . . . . . . . . . . . . . . . . . . . .     2.8
  Taper ratio . . . . . . . . . . . . . . . . . . . . . . . . . .     0.17
  Sweep angle, deg
    Leading edge  . . . . . . . . . . . . . . . . . . . . . . . .    51.7
    Quarter-chord line  . . . . . . . . . . . . . . . . . . . . .    45.4
    Trailing edge . . . . . . . . . . . . . . . . . . . . . . . .    14.2
Small-span trailing-edge flap
  Area, sq ft . . . . . . . . . . . . . . . . . . . . . . . . . .    25.81
  Flap span, percent wing semispan (21 to 46 percent) . . . . . .    25.0
  Chord, percent wing chord . . . . . . . . . . . . . . . . . . .    25.0
  Sweep angle of hinge line, deg  . . . . . . . . . . . . . . . .    26.8
Large-span trailing-edge flap
  Area, sq ft . . . . . . . . . . . . . . . . . . . . . . . . . .    41.14
  Flap span, percent wing semispan (21 to 66 percent) . . . . . .    45.0
  Chord, percent wing chord . . . . . . . . . . . . . . . . . . .    25.0
  Sweep angle of hinge line, deg  . . . . . . . . . . . . . . . .    26.8
Fuselage
  Length, ft  . . . . . . . . . . . . . . . . . . . . . . . . . .    48.0
  Maximum width, ft . . . . . . . . . . . . . . . . . . . . . . .     6.5
  Fineness ratio in wing chord plane  . . . . . . . . . . . . . .     7.4
Horizontal tail (drooped 20°)
  $S_t/S$ . . . . . . . . . . . . . . . . . . . . . . . . . . . .     0.192
  $b_t/b$ . . . . . . . . . . . . . . . . . . . . . . . . . . . .     0.53
  $l_t/\bar{c}$ . . . . . . . . . . . . . . . . . . . . . . . . .     1.52
  Aspect ratio  . . . . . . . . . . . . . . . . . . . . . . . . .     4.0
  Taper ratio . . . . . . . . . . . . . . . . . . . . . . . . . .     0.30
  Sweep angle of quarter-chord line, deg  . . . . . . . . . . . .    40.1
```

TABLE II.- COORDINATES OF BASIC WING

NACA 0005 (Modified) Section Parallel to the Model Plane of Symmetry			
Station, percent chord	Ordinate, percent chord	Station, percent chord	Ordinate, percent chord
0	0	30.00	2.501
1.25	.789	40.00	2.419
2.50	1.089	50.00	2.206
5.00	1.481	60.00	1.902
7.50	1.750	67.00	1.650
10.00	1.951	70.00	1.500
15.00	2.228	80.00	1.000
20.00	2.391	90.00	.500
25.00	2.476	100.00	0
Leading-edge radius: 0.275-percent c			

Plain Chord Extension Perpendicular to Leading Edge of Plain Wing	
Station, percent chord	Ordinate, percent chord
-4.83	0
-4.75	.23
-4.60	.39
-4.40	.53
-4.20	.64
-3.90	.78
-3.00	1.03
-2.00	1.15
-1.00	1.23
1.00	1.35
3.99	1.50

TABLE III.- COORDINATES OF MODIFIED LEADING-EDGE SECTIONS
PERPENDICULAR TO LEADING EDGE OF PLAIN WING

Modified Leading Edge on Wing		
Station, percent chord	Ordinate, percent chord	
	Upper surface	Lower surface
0	-0.60	-0.60
.05	-.29	-.89
.10	-.18	-1.01
.25	.07	-1.22
.50	.35	-1.42
.75	.53	-1.54
1.25	.80	-1.65
2.00	1.06	-1.71
2.50	1.21	-1.71
3.00	1.38	-1.70
3.50	1.42	-1.68
4.00	1.49	-1.67
4.50	1.57	-1.66
5.00	1.64	-1.64

Modified Leading Edge on Plain Chord Extension		
Station, percent chord	Ordinate, percent chord	
	Upper surface	Lower surface
-5.40	-0.60	-0.60
-5.30	-.17	-.99
-5.20	-.02	-1.16
-5.00	.21	-1.35
-4.60	.49	-1.55
-4.20	.67	-1.64
-3.60	---	-1.65
-3.20	.97	-1.62
-3.00	1.02	-1.61
-2.00	1.15	-1.46
-1.00	1.23	---
-.92	---	-1.24

CO████████

TABLE IV.- FUSELAGE COORDINATES

Station, ft	Diameter, ft	Elliptical cross section	
		Horizontal major axis, ft	Vertical minor axis, ft
0	2.96		
2.08	4.13		
4.58	4.82		
7.08	5.28		
9.58	5.60		
11.00	5.75		
12.00	5.83		
15.00	6.08		
18.00	6.33		
20.50	6.42		
23.00	6.50		
25.50	6.50		
28.00	6.50		
33.25	6.50		
35.67	6.33		
38.42		6.08	5.94
40.50		5.84	5.50
43.00		5.46	4.74
45.50		5.02	3.88
48.00		4.50	2.84

TABLE V.- MODEL CONFIGURATIONS FOR WHICH DATA ARE PRESENTED

Fig. no.	Data presented	Leading-edge flap δ_{le}, deg	Blowing extent, η	Nozzle	Extent of wing leading-edge modification	Trailing-edge flap, $\delta_{te} = 60°$ Span	Blowing
7	C_D, α, C_m variation with C_L	0,0,0[a] 0,0,0 0,40,50 30,60,60	None ↓ ↓ 0.4 - 1.0	None ↓ ↓ B	None	Small ↓	Off On ↓ On
8a		0,0,0 0,40,50 0,50,60 0,60,60 30,60,60	None	None			On
8b		0,0,0 0,40,50 0,50,50 0,50,60 0,60,60	None 0.4 - 1.0 ↓	None A ↓			
8c		0,0,0 0,40,50 0,50,60 0,60,60 30,60,60	None 0.4 - 1.0 ↓	None B ↓			
8d		30,60,60 50,60,60	0.4 - 1.0 0.15 - 1.0	B	0.4 - 1.0		
9a		0,50,60	0.7 - 1.0 0.7 - 1.0 0.4 - 1.0 0.4 - 1.0	A B A B	None		
9b		0,60,60	0.4 - 1.0	A & B			
9c		30,60,60		B	↓		
10a		30,60,60	0.4 - 1.0	B	0.7 - 1.0		
10b					0.4 - 1.0		↓
11a		0,0,0[a] 0,0,0 0,0,0 30,60,60 30,60,60	None 0.4 - 1.0	None B	None		Off Off On Off On
11b		0,0,0[a] 0,0,0 0,0,0 30,60,60 30,60,60	None 0.4 - 1.0	None B		Large ↓	Off Off On Off On
12a	C_L variation with $C_{\mu_{le}}$	30,60,60	0.4 - 1.0	A & B		Small ↓	On
12b				B			
13				A			
14				B			
17a	C_L variation with $C_{\mu_{te}}$	0,40,50	None	None		↓	
17b		30,60,60	0.4 - 1.0	B	↓	Large	↓

[a] $\delta_{te} = 0°$

A-22148

Figure 1.- Photograph of model in the Ames 40- by 80-foot wind tunnel.

34

CONFIDENTIAL

NACA RM A58A09

75-percent c line
(hinge line for
T.E. flaps)

3.18

Horizontal-tail
reference line, $\bar{c}/4$

10.59

19.43

45.4°

$\bar{c} = 12.77$

15.31

6.50

8.06

5.84

L.E. flap
breaks at
η, .15, .40 &
.70

44.4°

12.20

25-percent c line

12-percent c
line (hinge line
for L.E. flap)

10-percent c plain chord
extension
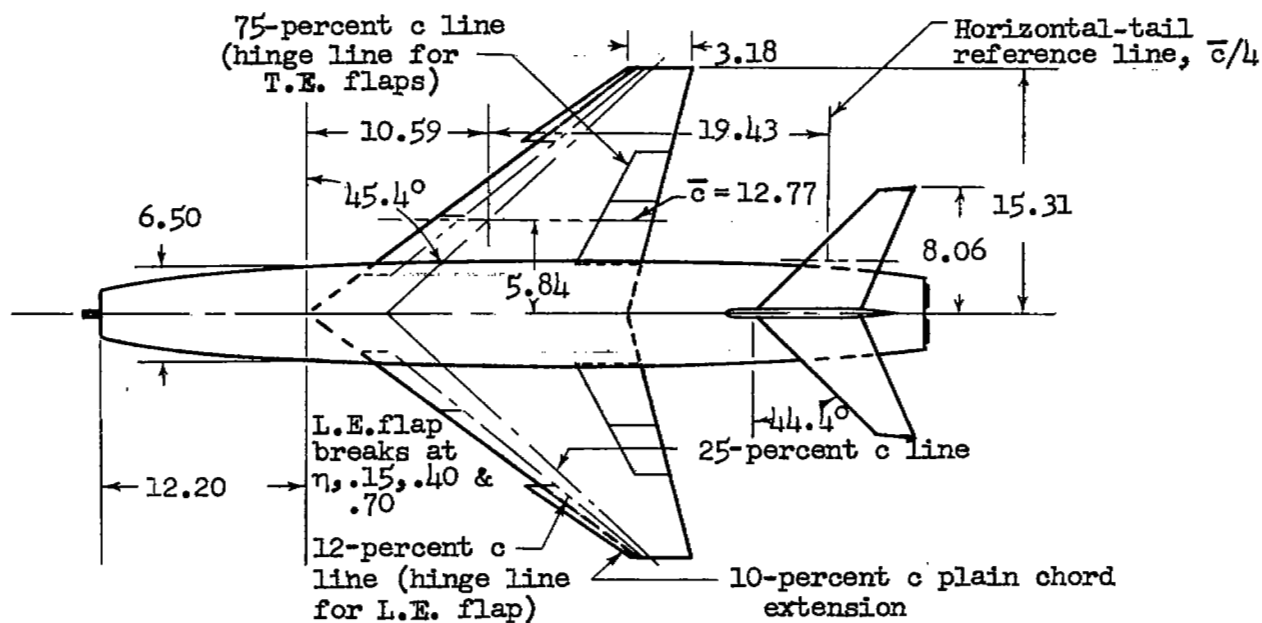
All dimensions in feet,
unless otherwise noted

$\bar{c} = 7.47$

4.12

45°

10.30

2.73

1.98

4.43

Horizontal tail
drooped 20°

10.00

48.00
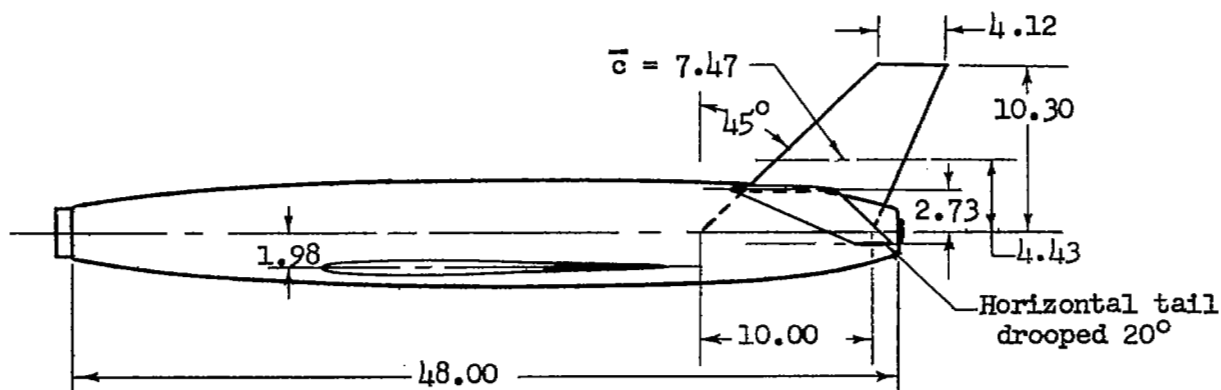
Figure 2.- Dimensional details of the model.

CONFIDENTIAL

.010 inch from η=0.15-.7
.010 or .050 inch from
     η=0.7-1.0

35.5°

δ_{le}

Air flow

Hinge line
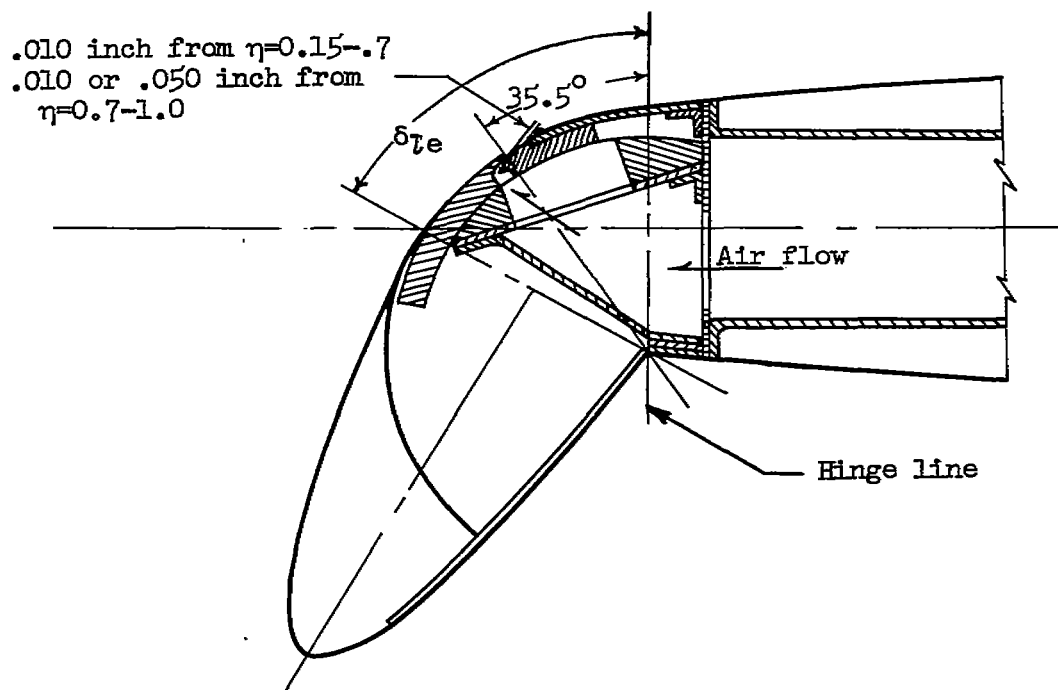
(a) Typical leading-edge-flap cross section.

22.5° δ_{te} 0.020 inch

Air flow

Hinge line
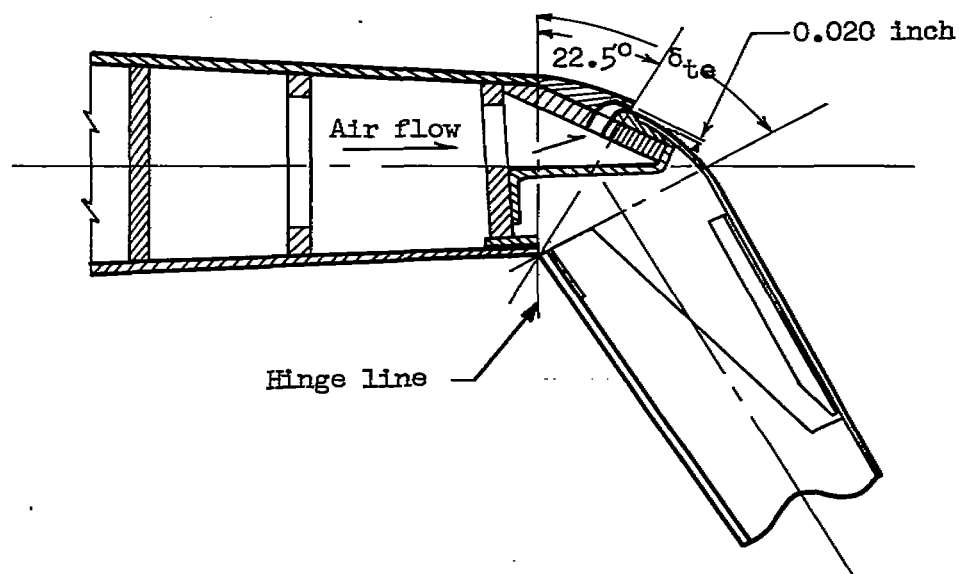
(b) Typical trailing-edge-flap cross section.

Figure 3.- Blowing nozzle arrangements of three-dimensional model.

Plain L.E.

Wing L.E. (ref)

.9

L.E. flap chord plane

.6

Modified L.E.,L.E. radius .9

Center, L.E. arc

Hinge point of L.E. flap

(a) η = 0.4 to 0.7

L.E. flap chord plane

Plain chord extension

.33

.6

4.83

Wing L.E. (ref)

Chord with modified L.E.
L.E. radius .9

Center of L.E. arc

Hinge point of L.E. flap
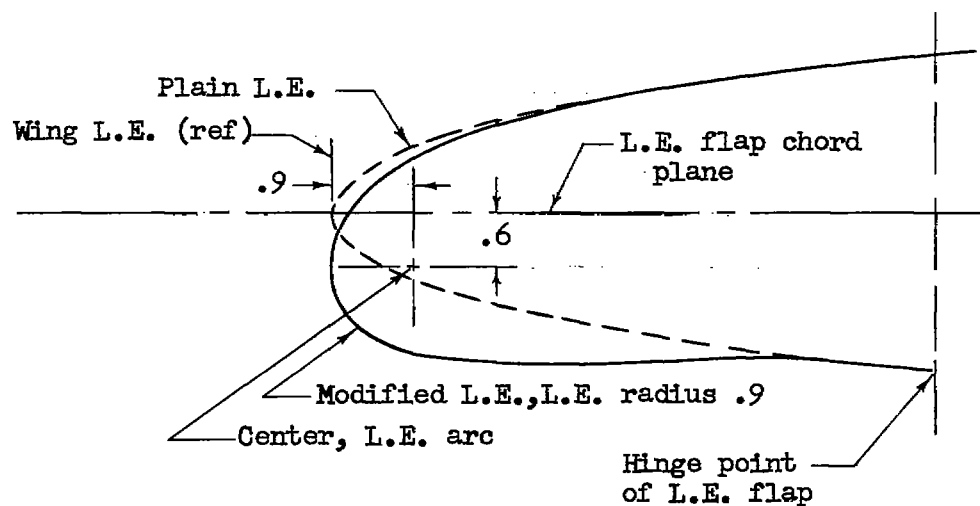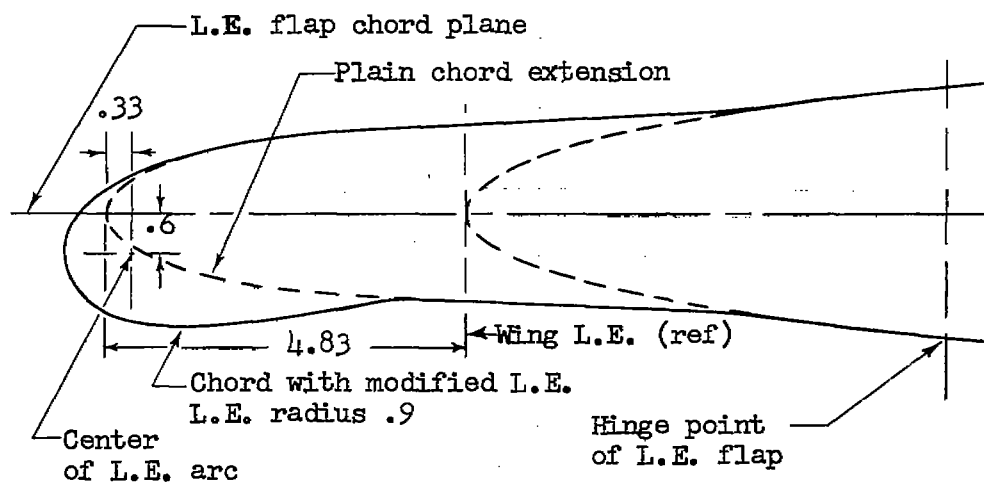
(b) η = 0.7 to 1.0

Figure 4.- Leading-edge modification used in the investigation. All sections perpendicular to the wing leading edge. Dimensions in percent chord.
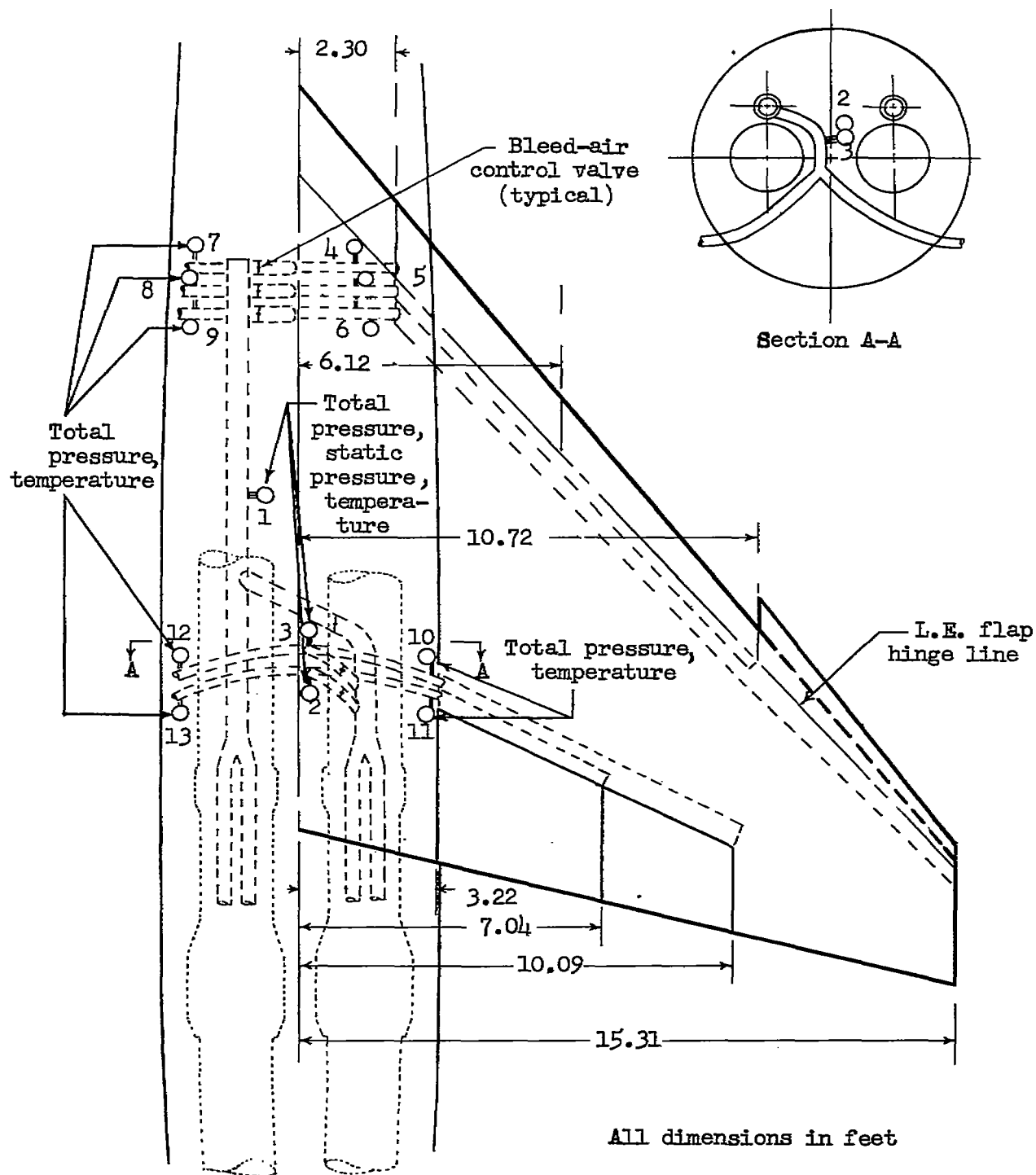
Figure 5.- Sketch of bleed-air ducting.

Station, percent c	Ordinate, percent c
0	0
.50	.80
.75	.97
1.25	1.22
2.50	1.69
5.00	2.33
7.50	2.81
10.00	3.19
15.00	3.81
20.00	4.27
25.00	4.60
30.00	4.83
35.00	4.96
40.00	5.00
45.00	4.89
50.00	4.69
55.00	4.38
60.00	4.02
65.00	3.60
70.00	3.13
80.00	2.10
90.00	1.06
100.00	.02
L.E. radius: 0.69	
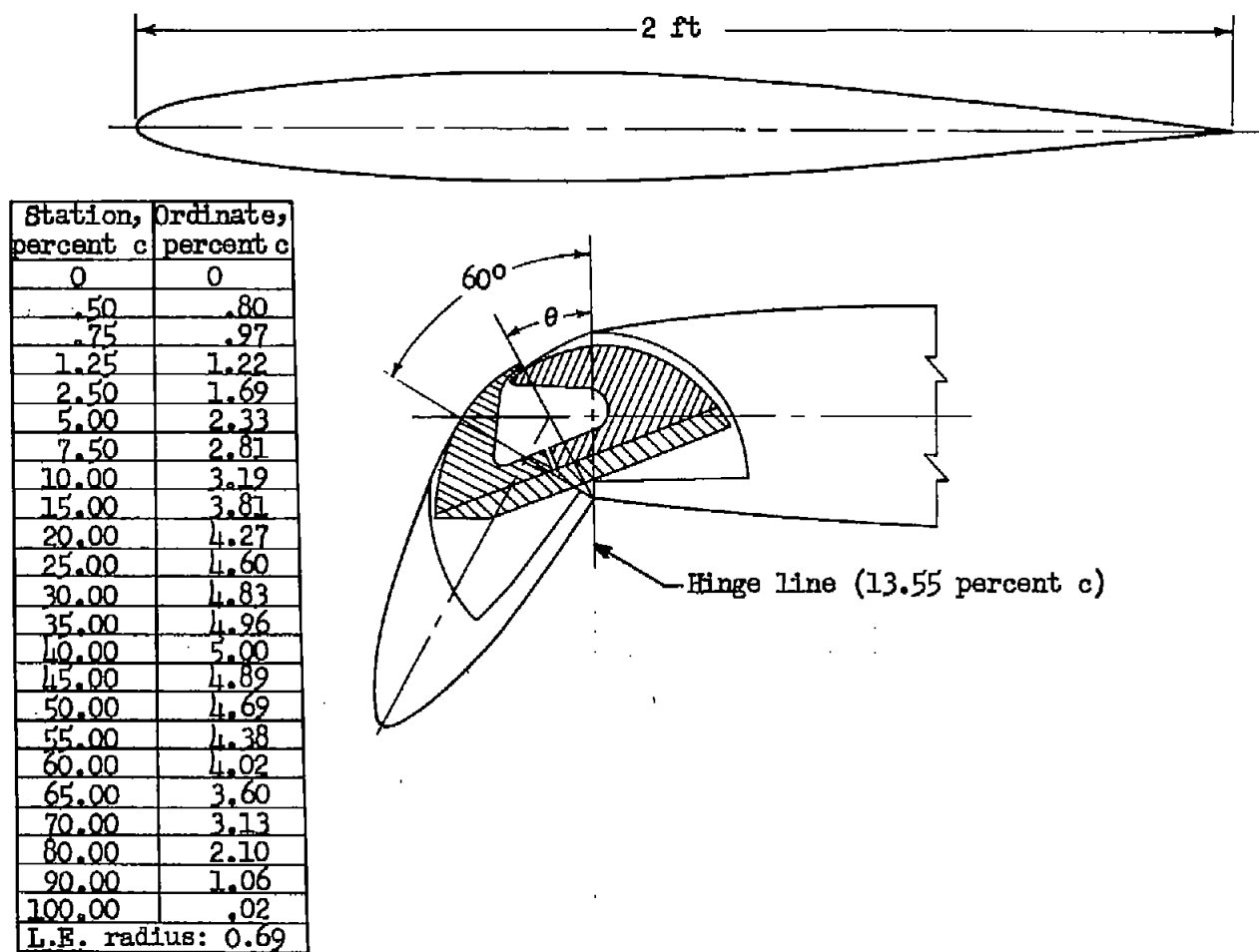
Figure 6.- Details of the two-dimensional blowing model.

	δ_{le},deg	δ_{te},deg	$C_{\mu le}$	$C_{\mu te}$
o	0, 0, 0	0	0	0
□	0, 0, 0	60	0	0.006
◇	0,40,50	60	0	.006
△	30,60,60	60	0.076	.006
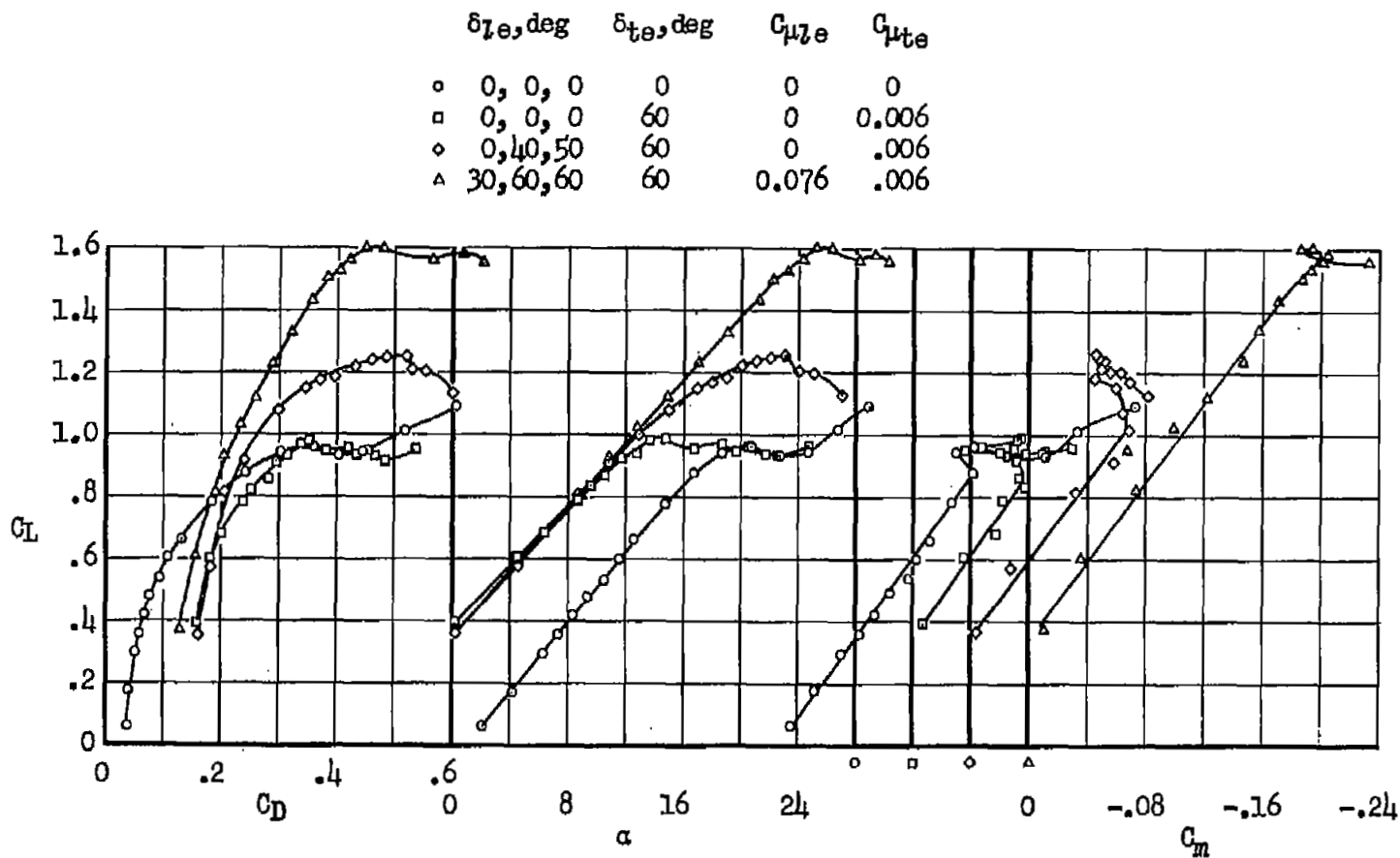
Figure 7.- The effect of BLC on the longitudinal characteristics of the model; small-span trailing-edge flap.
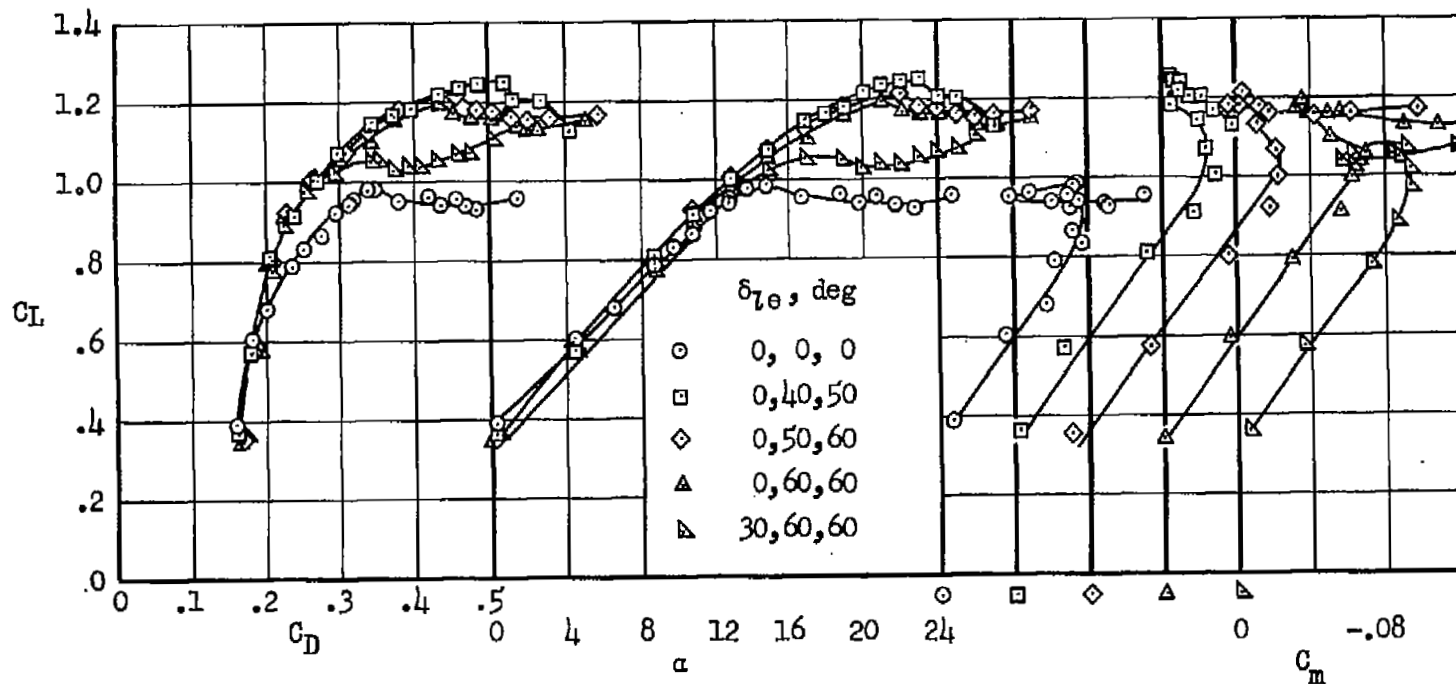
(a) $C_{\mu_{le}} = 0$

Figure 8.- Longitudinal characteristics for several leading-edge flap configurations with and without leading-edge BLC; small-span trailing-edge flap, $\delta_{t_e} = 60°$, $C_{\mu_{te}} = 0.006$.
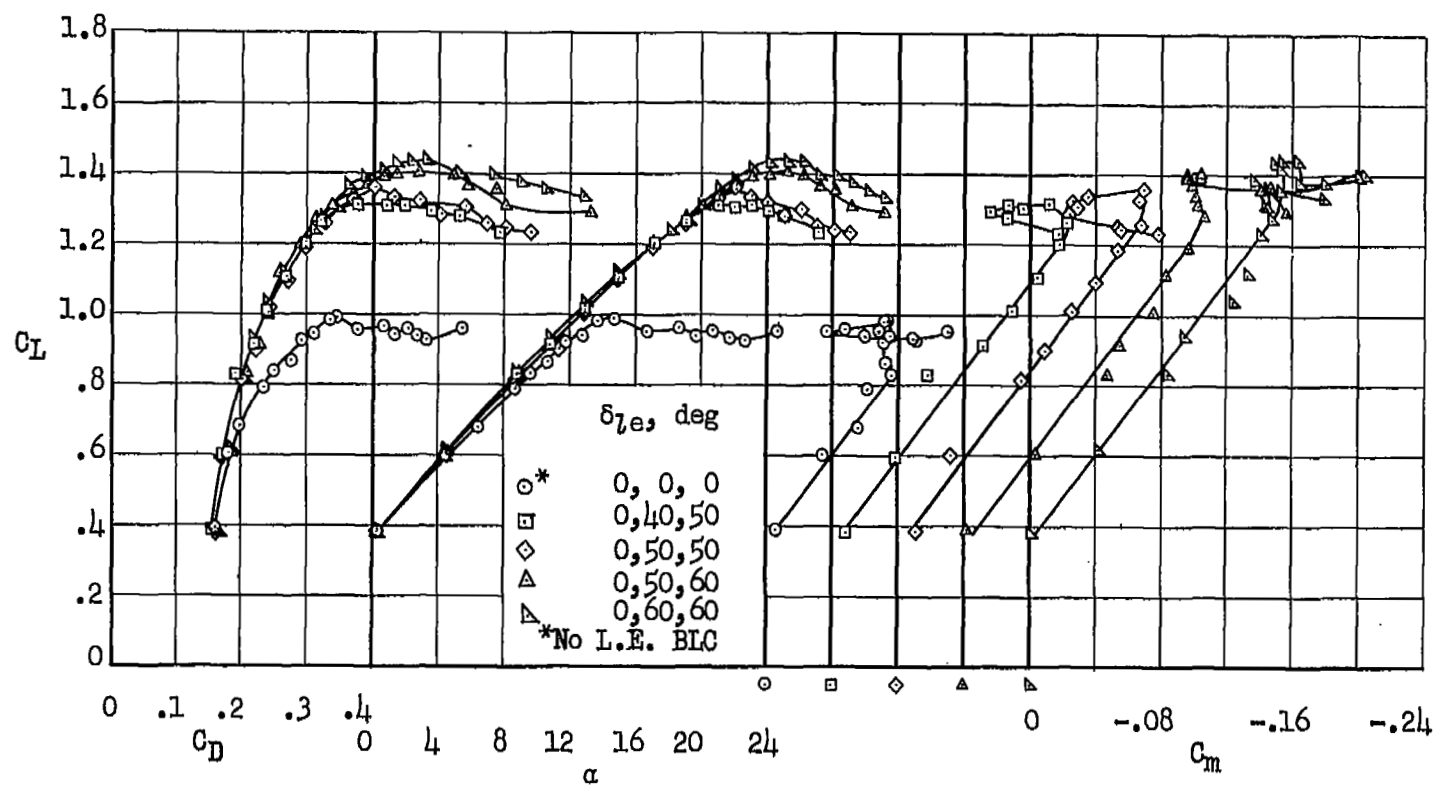
(b) Leading-edge BLC with nozzle A; $C_{\mu le} = 0.027$.

Figure 8.- Continued.

Legend:

δ_{le}, deg

⊙*	0, 0, 0
▢	0,40,50
◇	0,50,60
△	0,60,60
◁	30,60,60

*No L.E. BLC

C_L

C_D α C_m
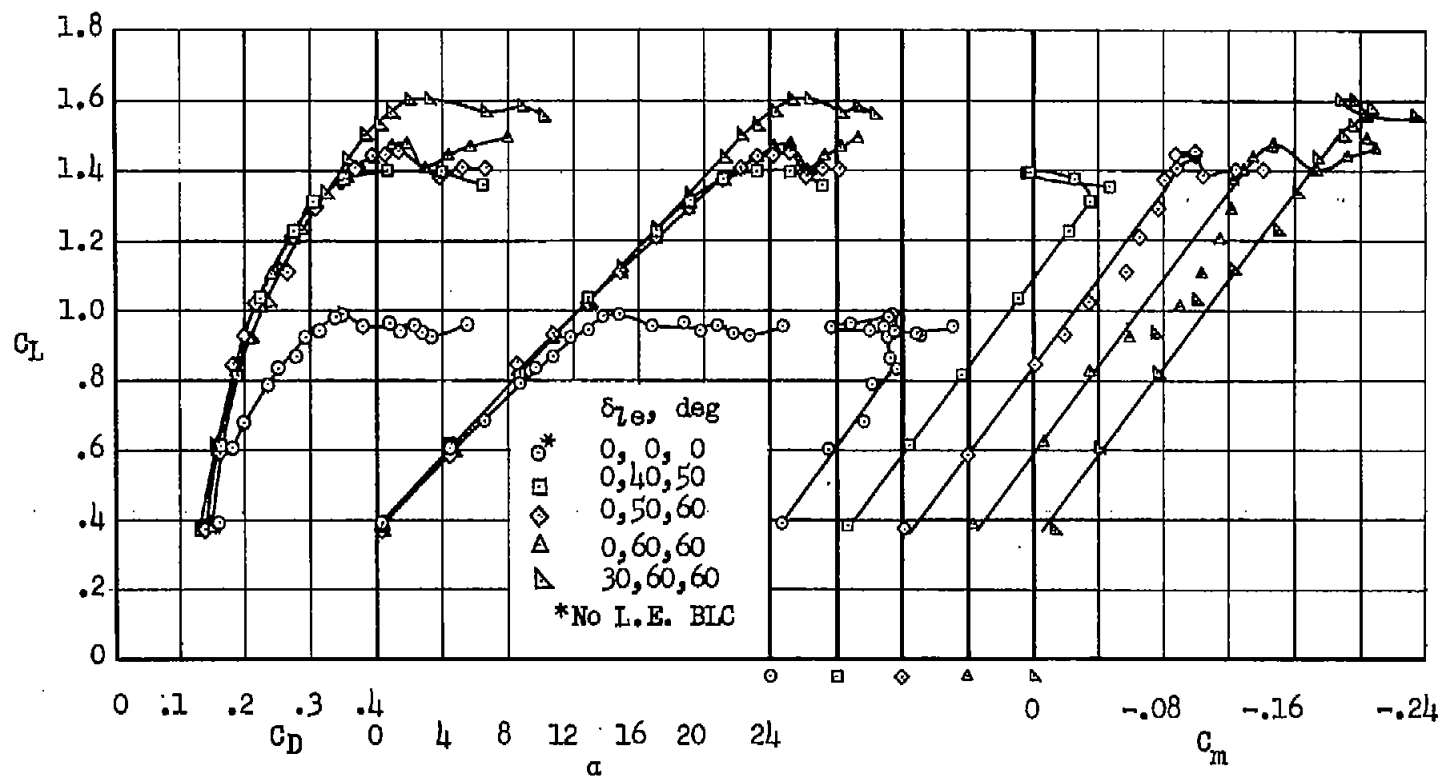
(c) Leading-edge BLC with nozzle B; $C_{\mu le} = 0.076$.

Figure 8.- Continued.
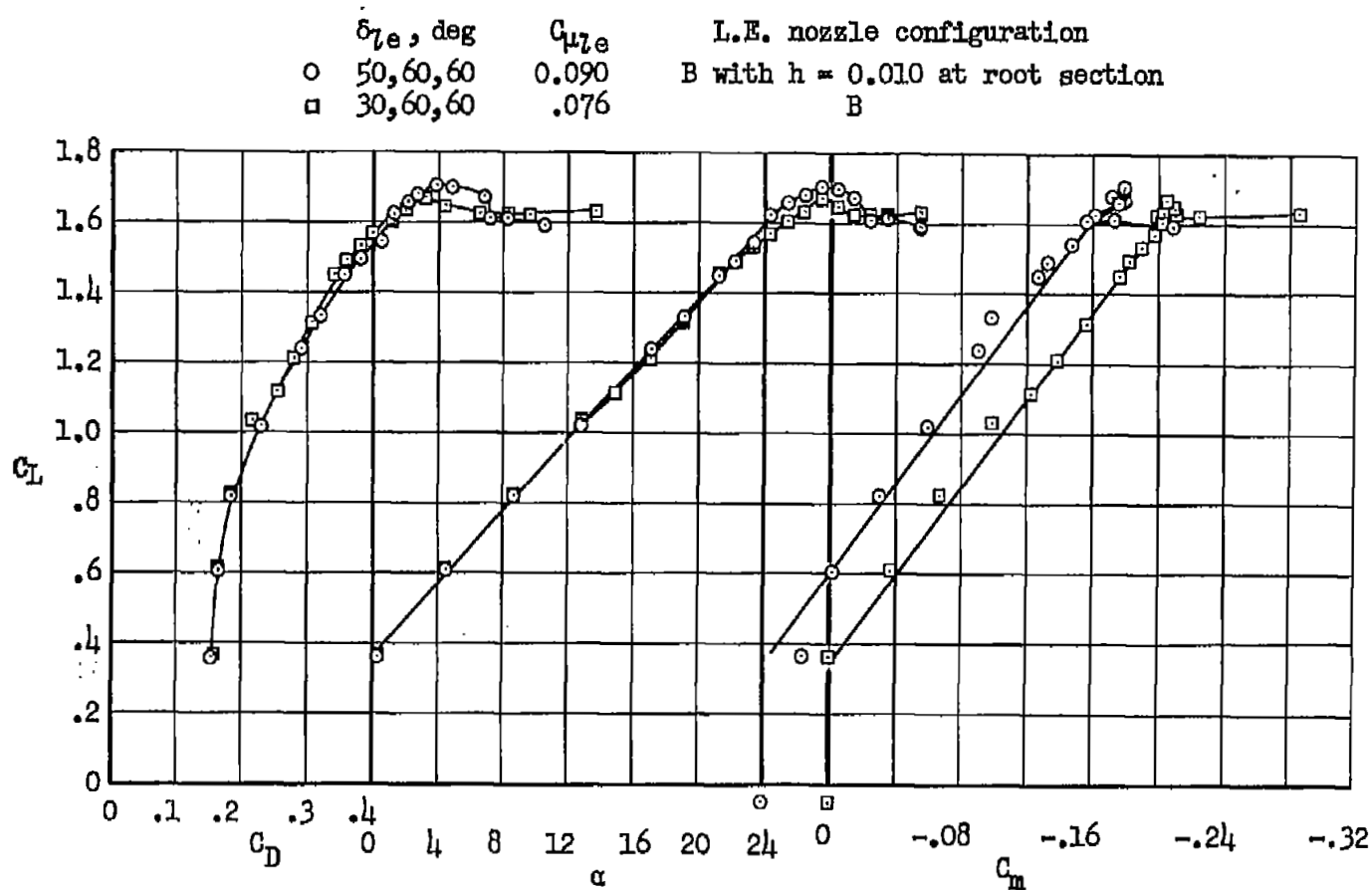
(d) Effect of root flap deflection with the modified leading edge from η = 0.4 to 1.0.

Figure 8.- Concluded.

	$C_{\mu le}$	LE nozzle	Extent of blowing, η	LE h from $\eta = 0.7$–1.0
○	0	– –	– –	– –
▫	0.011	– –	.7–1.0	0.010
◇	.057	– –	.7–1.0	.050
△	.027	A	.4–1.0	.010
▲	.074	B	.4–1.0	.050
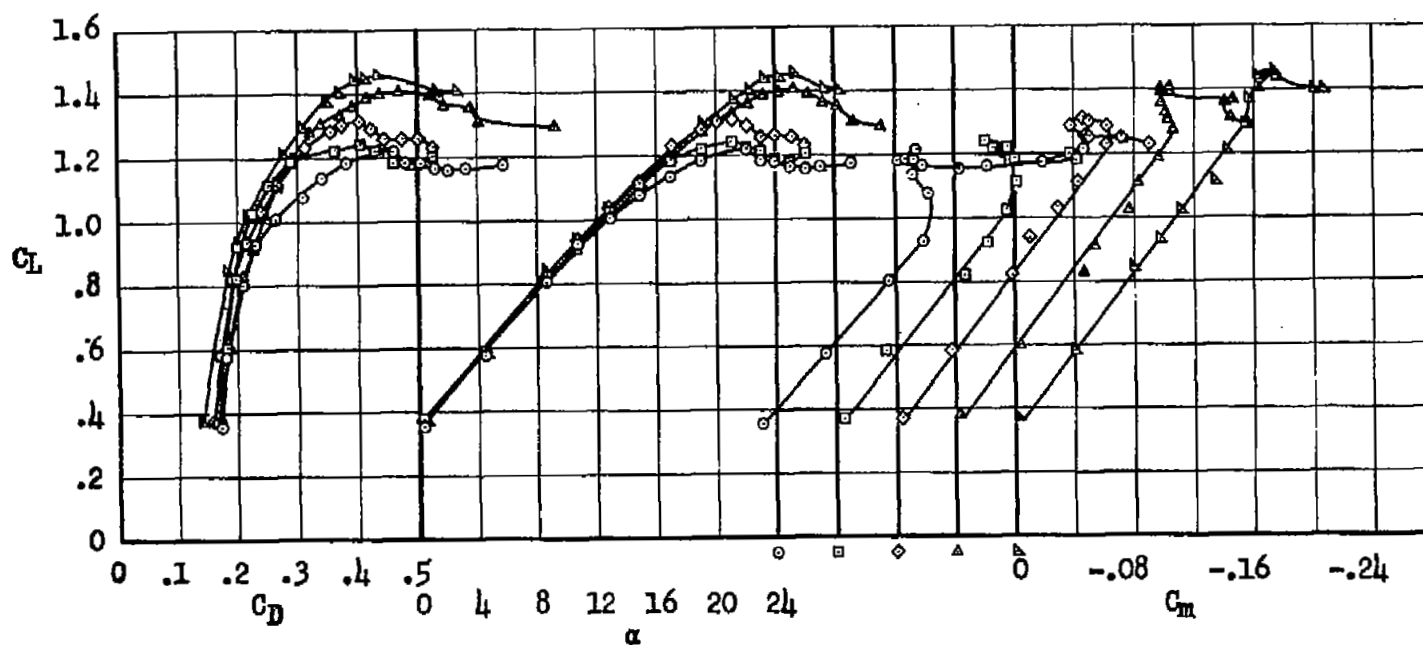
(a) Effect of blowing on the intermediate flap section; $\delta_{le} = 0, 50, 60$.

Figure 9.- Longitudinal characteristics with different amounts and spanwise extents of blowing BLC on the leading edge; small-span trailing-edge flap, $\delta_{te} = 60°$, $C_{\mu te} = 0.006$.
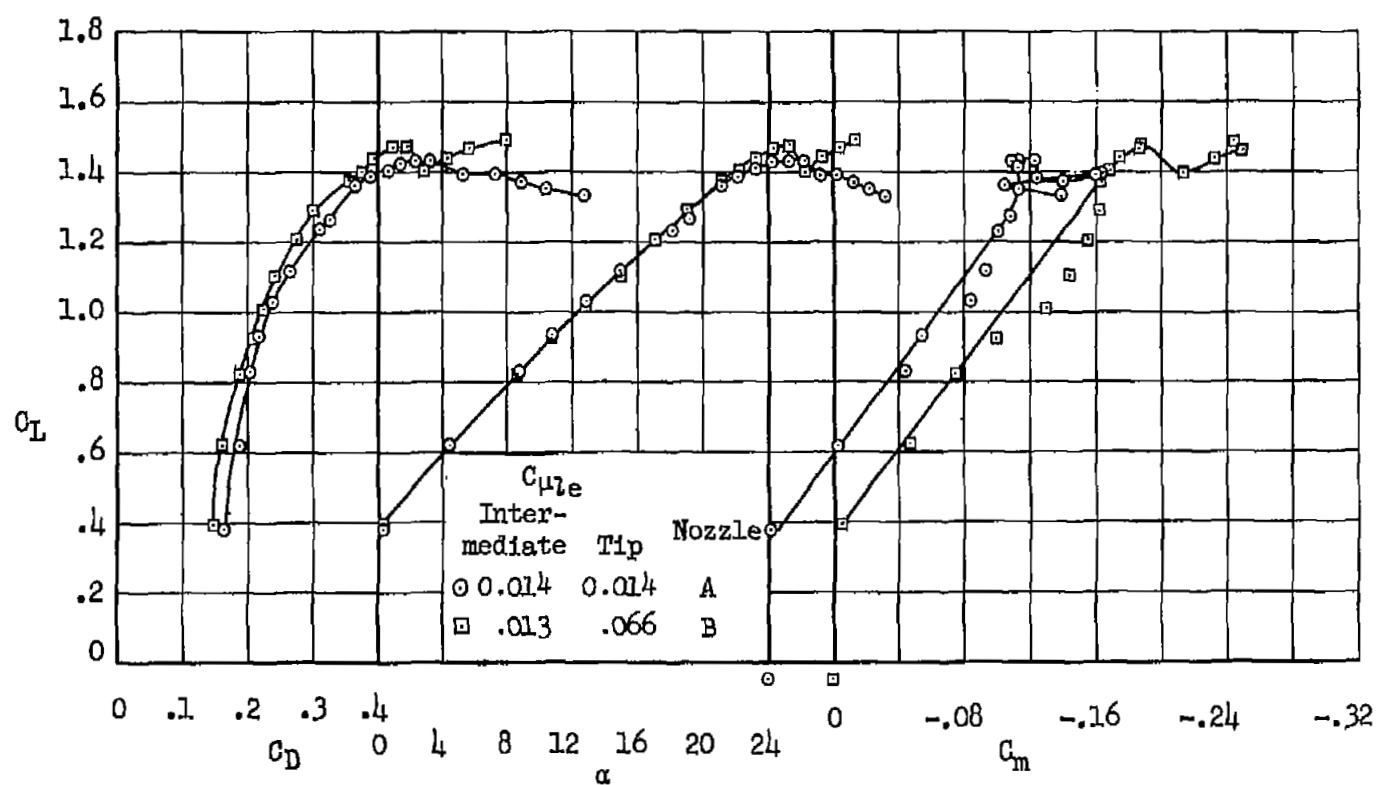
(b) Effect of increased blowing from η = 0.7 to 1.0; δ_le = 0,60,60.

Figure 9.- Continued.
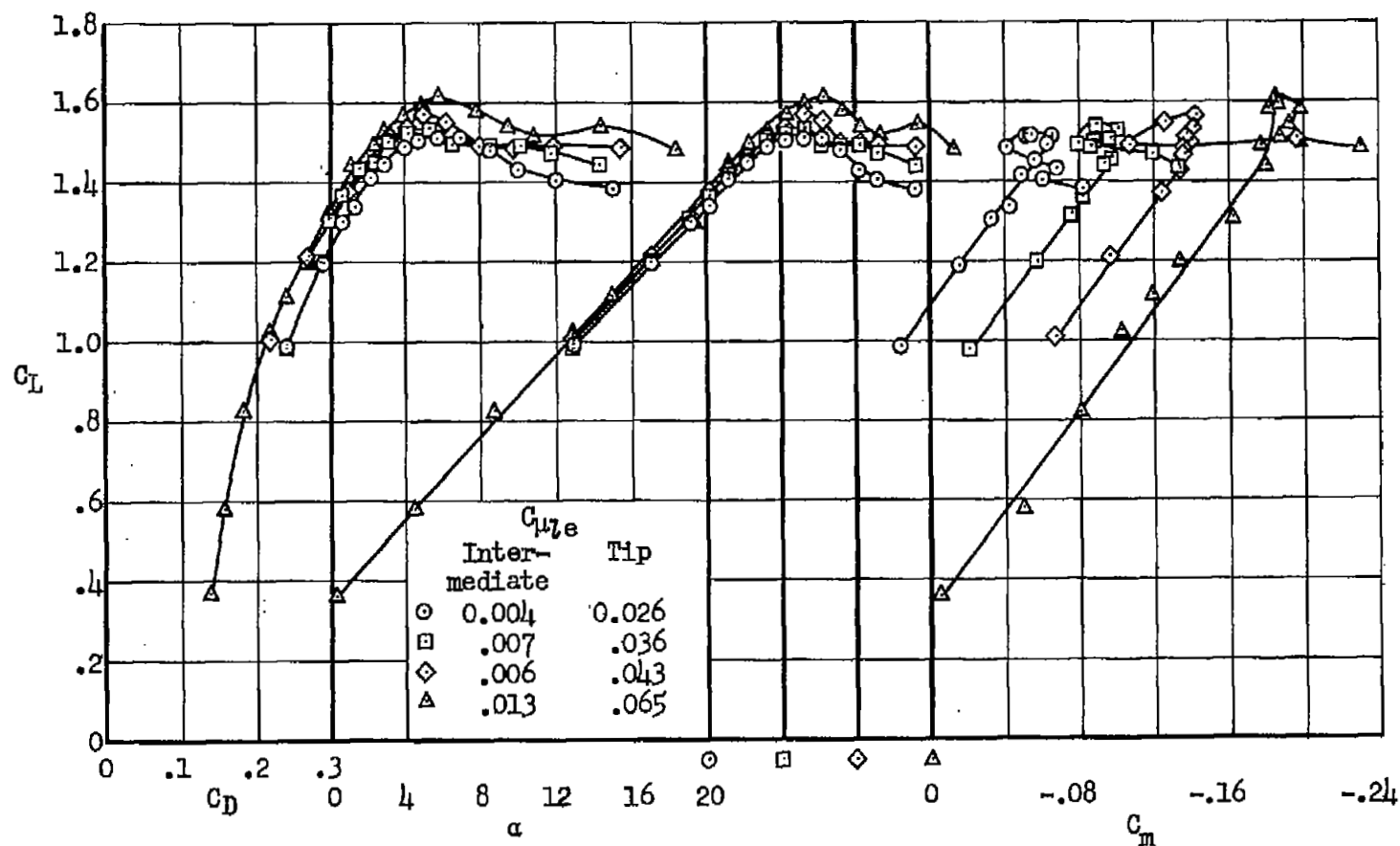
(c) Effect of changing total C_μ, nozzle B; $\delta_{le} = 30,60,60$.

Figure 9.- Concluded.
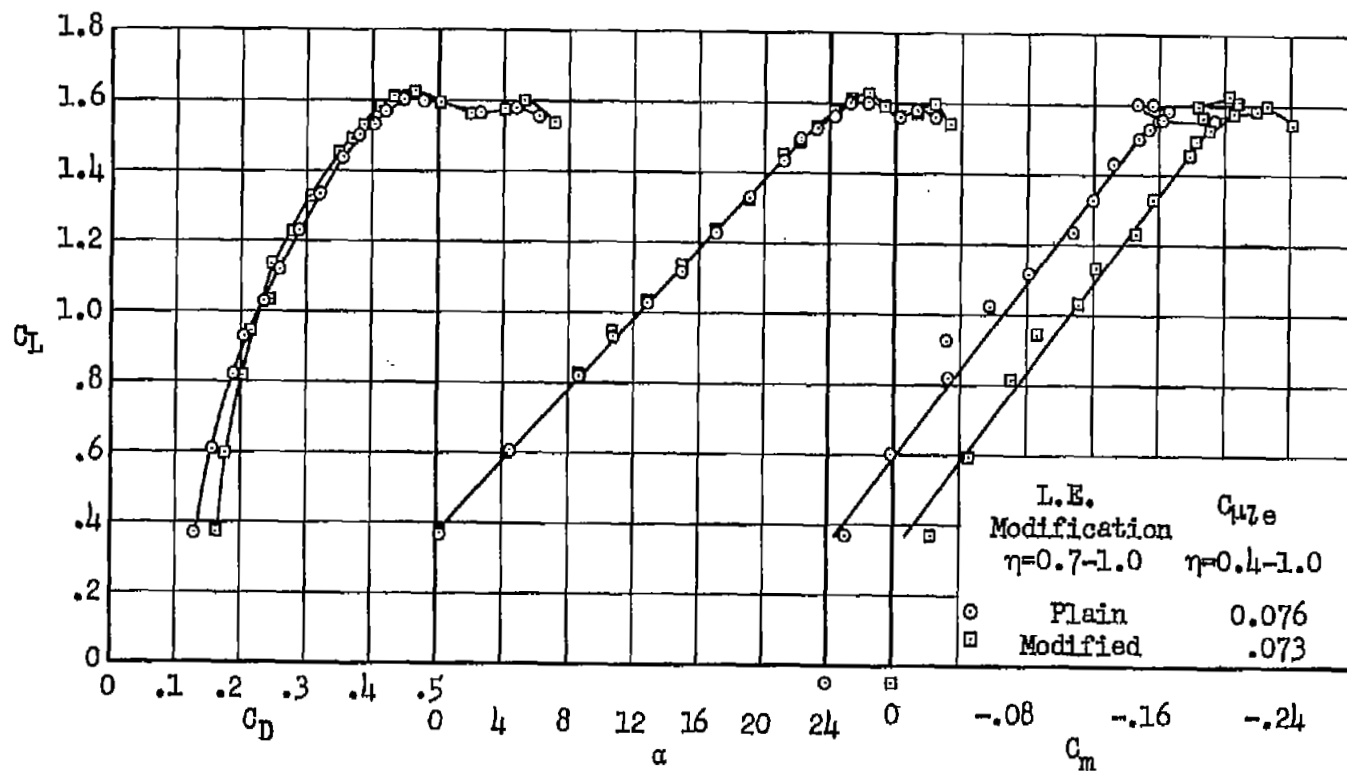
(a) Effect of applying the modified leading edge from $\eta = 0.7$ to 1.0.

Figure 10.- Effect of the modified leading edge on longitudinal characteristics; $\delta_{le} = 30,60,60$, leading-edge nozzle B, small-span trailing-edge flap, $\delta_{te} = 60°$, $C_{\mu te} = 0.006$.
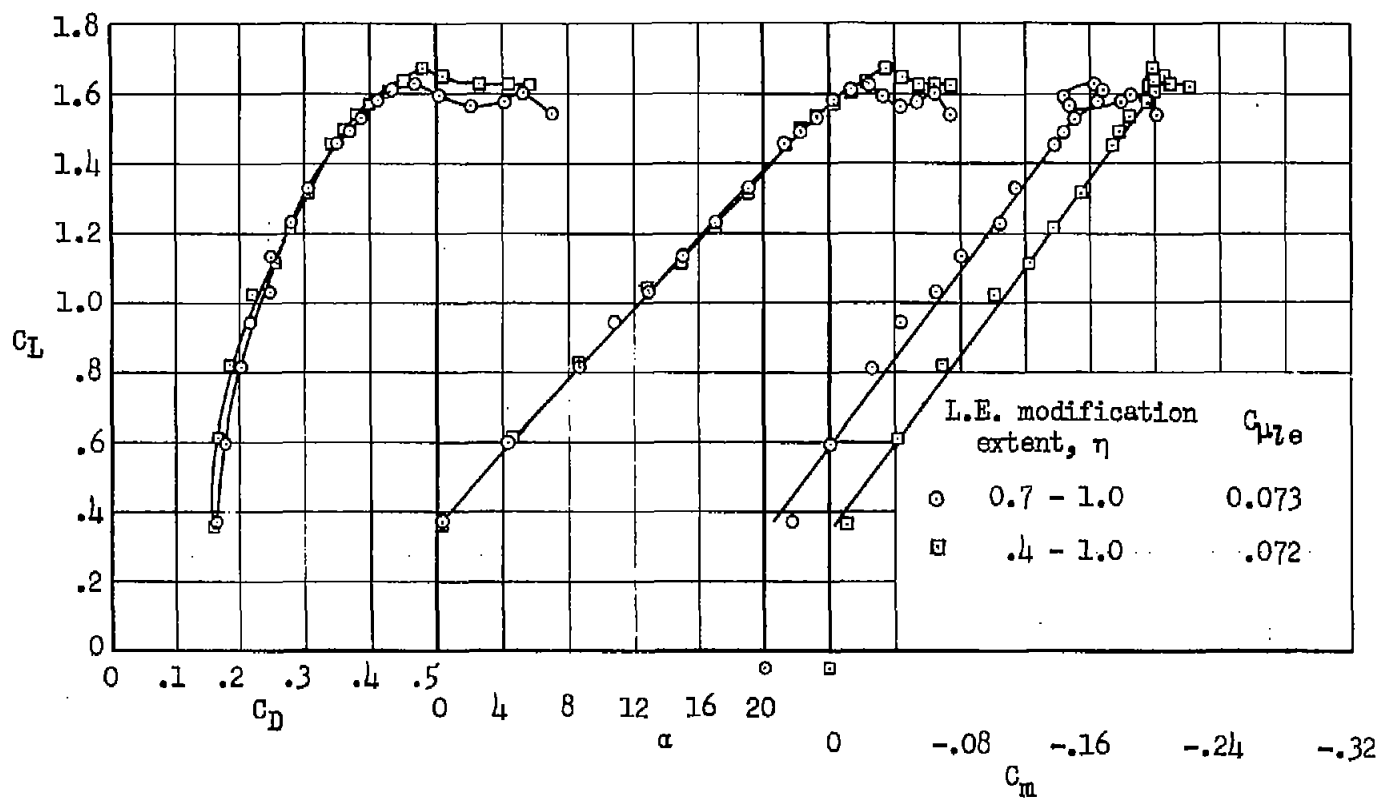
(b) Effect of increasing the spanwise extent of modified leading edge.

Figure 10.- Concluded.

δ_{le},deg	$C_{\mu_{le}}$	$C_{\mu_{te}}$
o *0, 0, 0	0	0
□ 0, 0, 0	0	0
◇ 0, 0, 0	0	0.006
△ 30,60,60	0.074	0
▲ 30,60,60	.076	.006

*$\delta_{te} = 0^{o}$
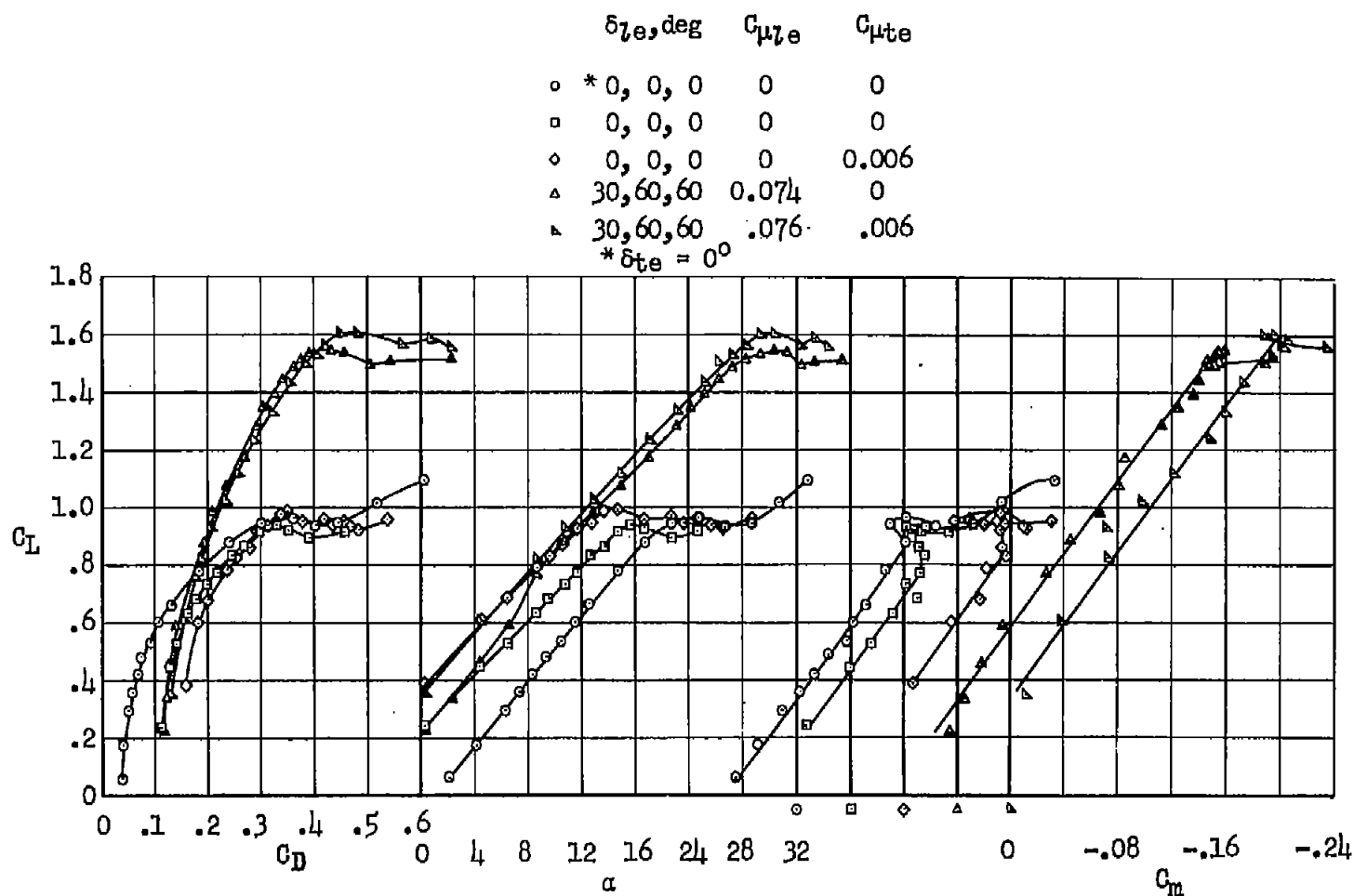
(a) Small-span trailing-edge flap.

Figure 11.- Effect of trailing-edge flap on the longitudinal characteristics of the model with and without leading-edge BLC; nozzle B with leading-edge BLC, $\delta_{te} = 60^{o}$.
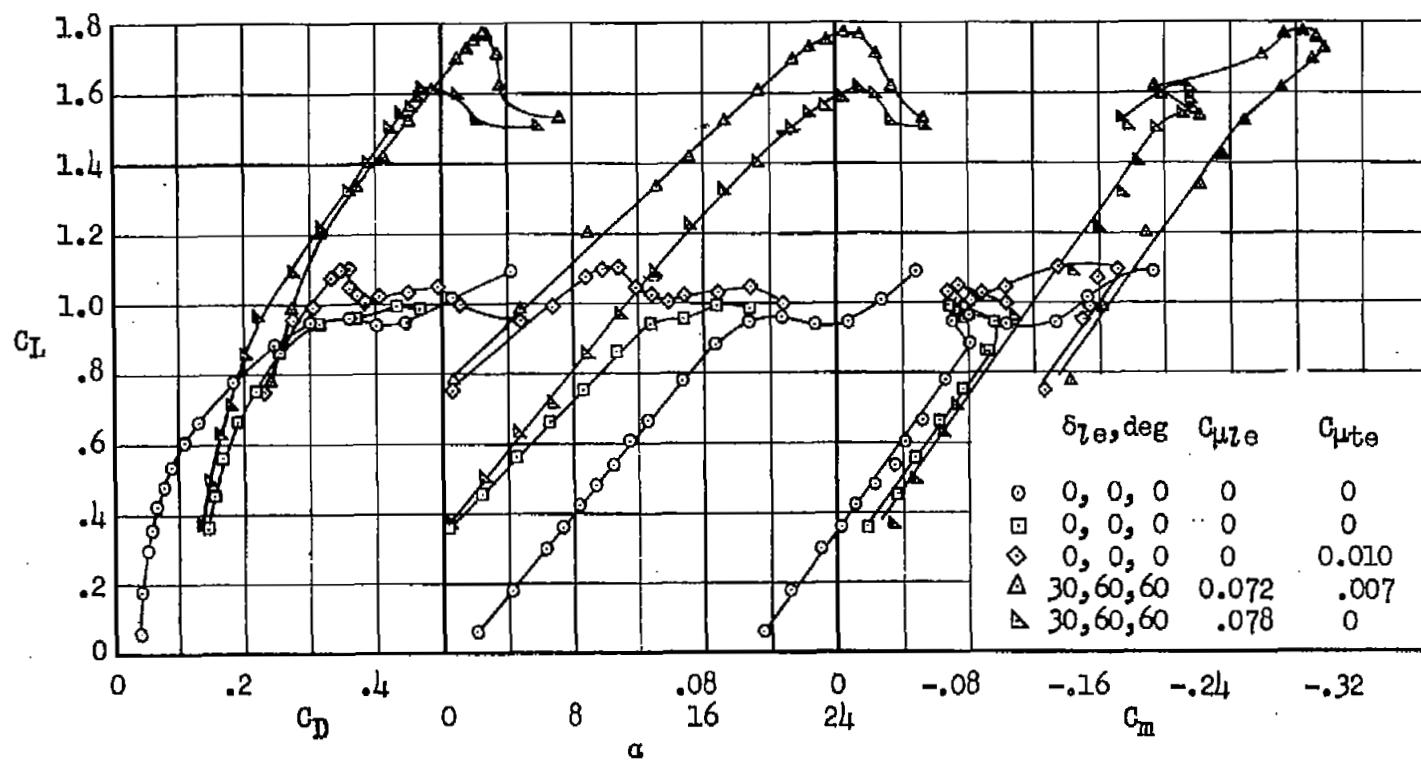
(b) Large-span trailing-edge flap.

Figure 11.- Concluded.
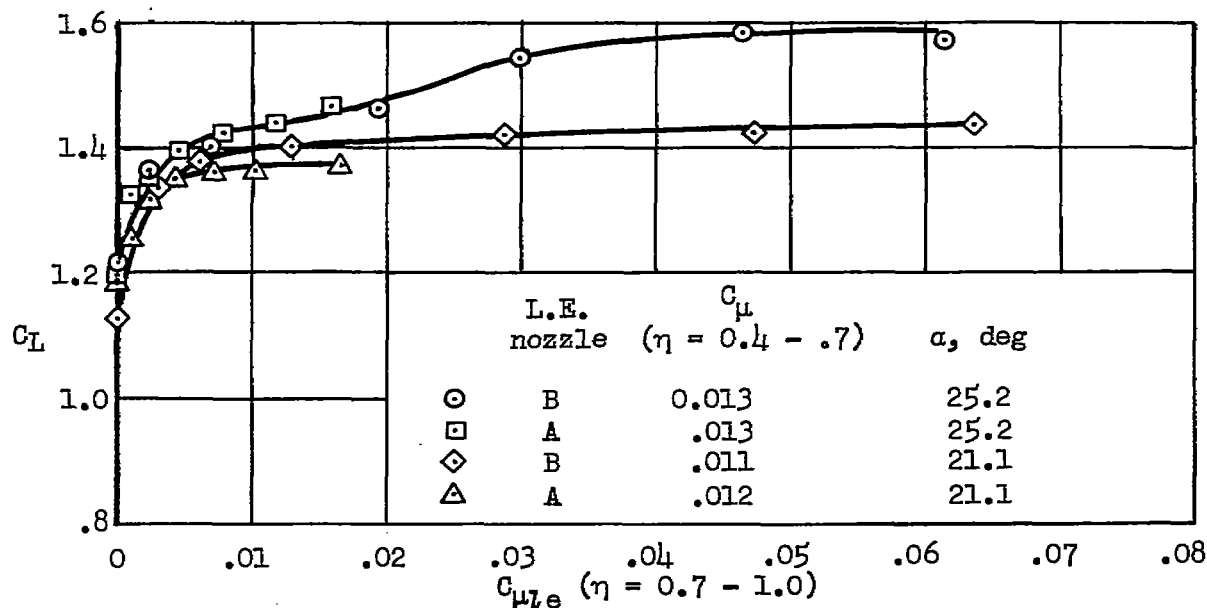
(a) Effect of nozzle height.
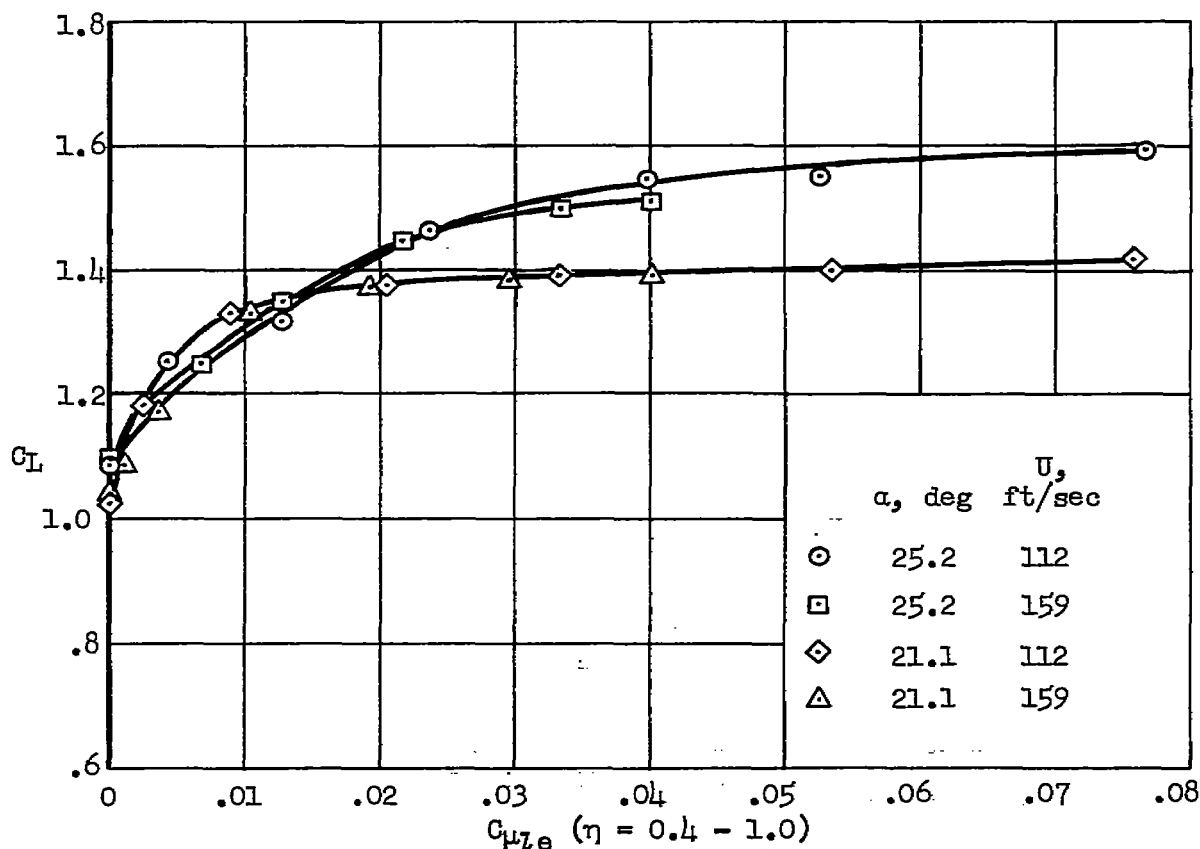
(b) Effect of free-stream air velocity; leading-edge nozzle B.

Figure 12.- Variation of lift with leading-edge C_μ; $\delta_{le} = 30,60,60$, small span flap, $\delta_{te} = 60°$, $C_{\mu te} = 0.006$.
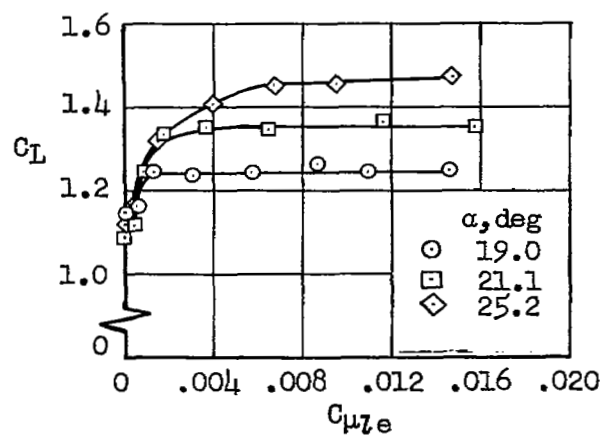
(a) $\eta = 0.4$ to 0.7 ($\eta = 0.7$ to 1.0 $C_{\mu l e} = 0.015$)
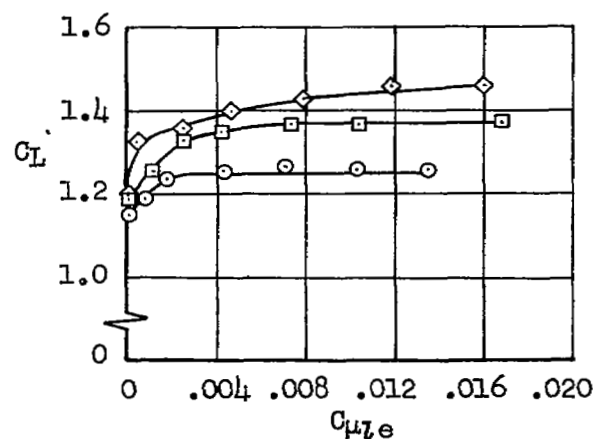
(b) $\eta = 0.7$ to 1.0 ($\eta = 0.4$ to 0.7 $C_{\mu l e} = 0.013$)
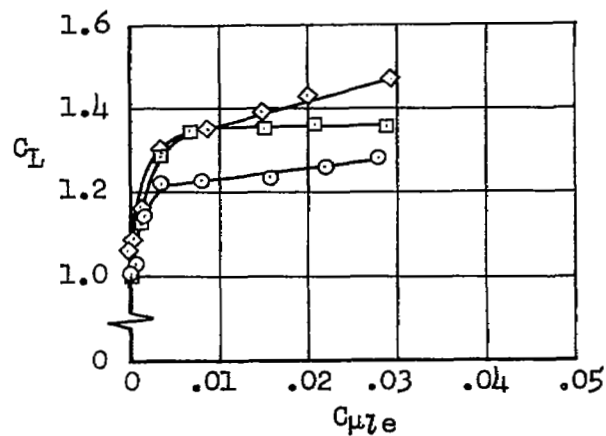
(c) $\eta = 0.4$ to 1.0

Figure 13.- Effect of angle of attack on the variation of lift with $C_{\mu l e}$; $\delta_{l e} = 30,60,60$, leading-edge nozzle A, small-span trailing-edge flap, $\delta_{te} = 60°$, $C_{\mu te} = 0.006$.
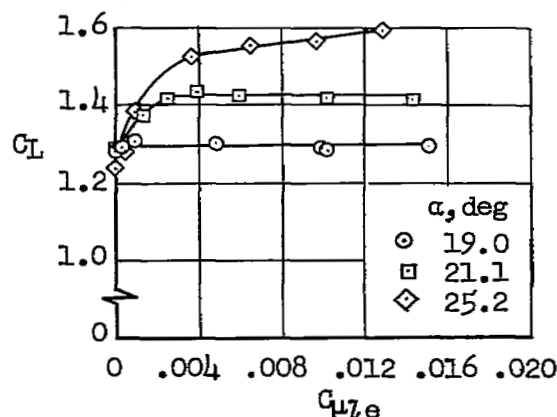
(a) $\eta = 0.4$ to 0.7 ($\eta = 0.7$ to 1.0 $C_{\mu le} = 0.060$)
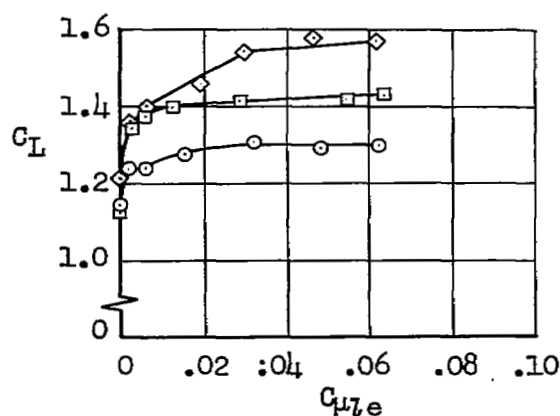
(b) $\eta = 0.7$ to 1.0 ($\eta = 0.4$ to 0.7 $C_{\mu le} = 0.011$)
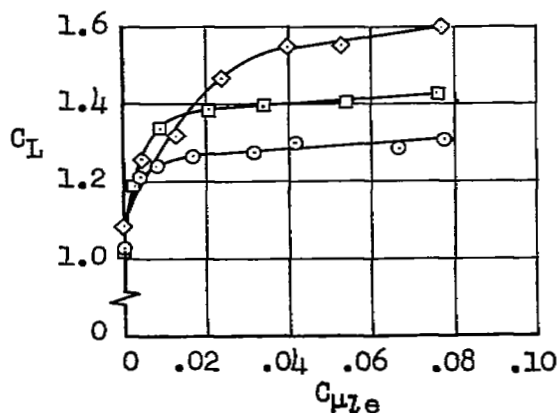
(c) $\eta = 0.4$ to 1.0

Figure 14.- Effect of angle of attack on the variation of lift with $C_{\mu le}$, $\delta_{le} = 30,60,60$, leading-edge nozzle B, small-span trailing-edge flap, $\delta_{te} = 60°$, $C_{\mu te} = 0.006$.
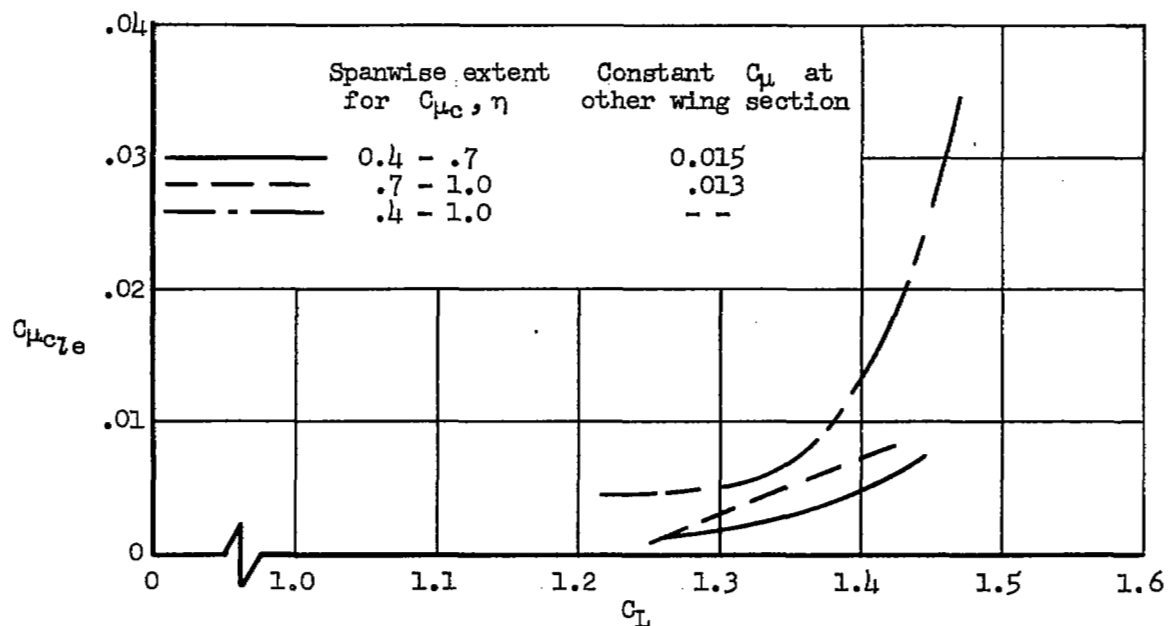
(a) Leading-edge nozzle A.
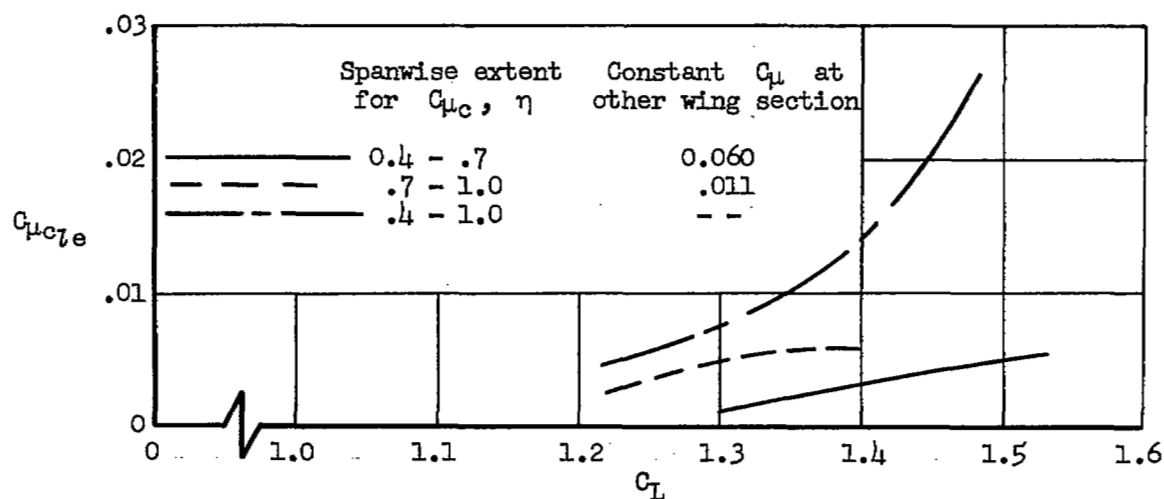
(b) Leading-edge nozzle B.

Figure 15.- Variation of $C_{\mu c_{l e}}$ with C_L, $\delta_{l e}$ = 30,60,60; small-span
trailing-edge flap, δ_{te} = 60°, $C_{\mu te}$ = 0.006.
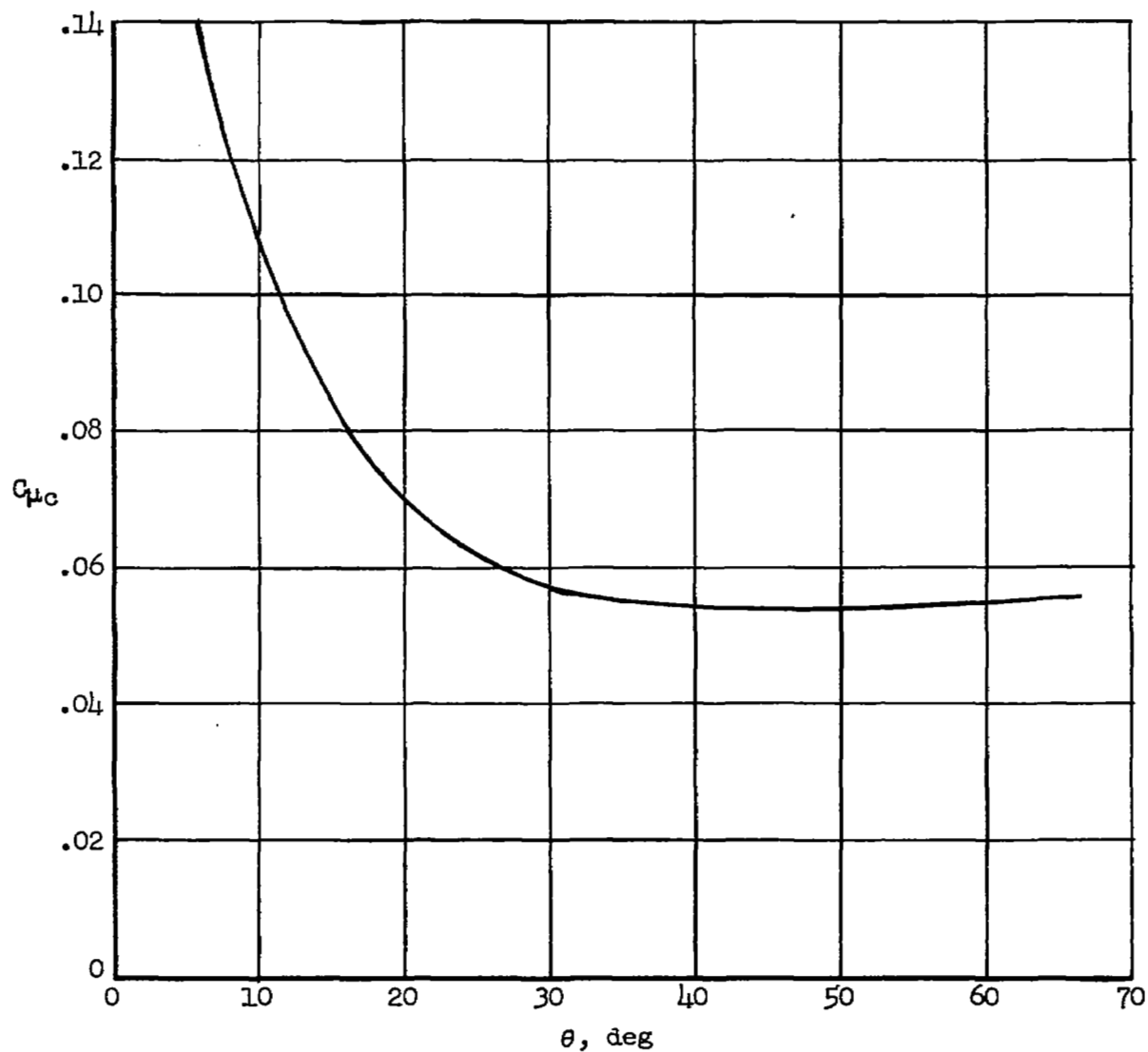
Figure 16.- Effect of leading-edge nozzle location on $C_{\mu c_{le}}$; two-dimensional data, $R = 1.65\times10^6$, $\delta_{le} = 60^\circ$, $\alpha = 36^\circ$, h/c = 0.00033.
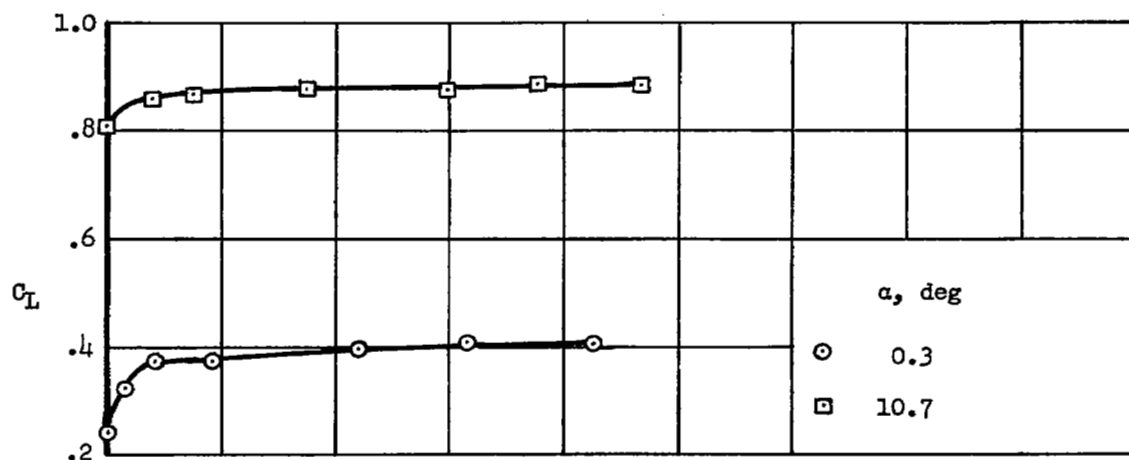
(a) Small-span flap, δ_{le} = 0,40,50, without leading-edge BLC.
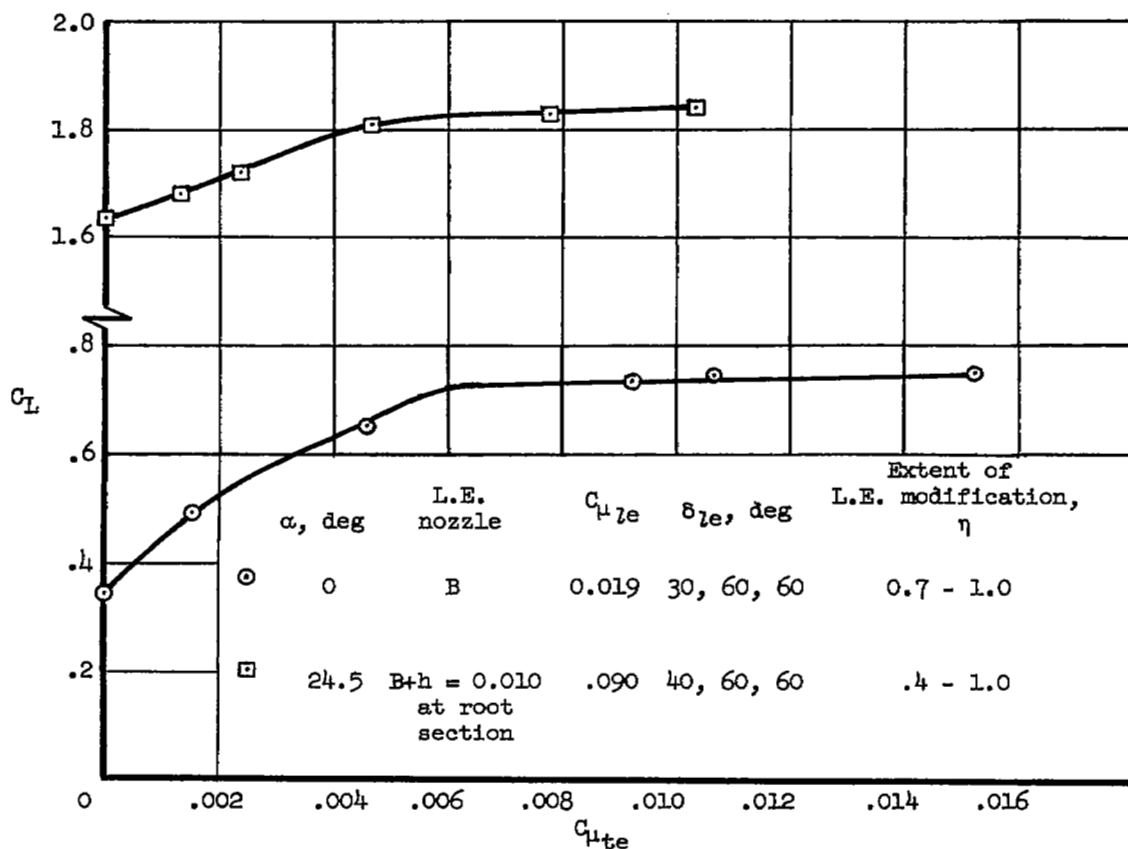
(b) Large-span flap.

Figure 17.- Variation of lift coefficient with $C_{\mu te}$, δ_{te} = 60°.
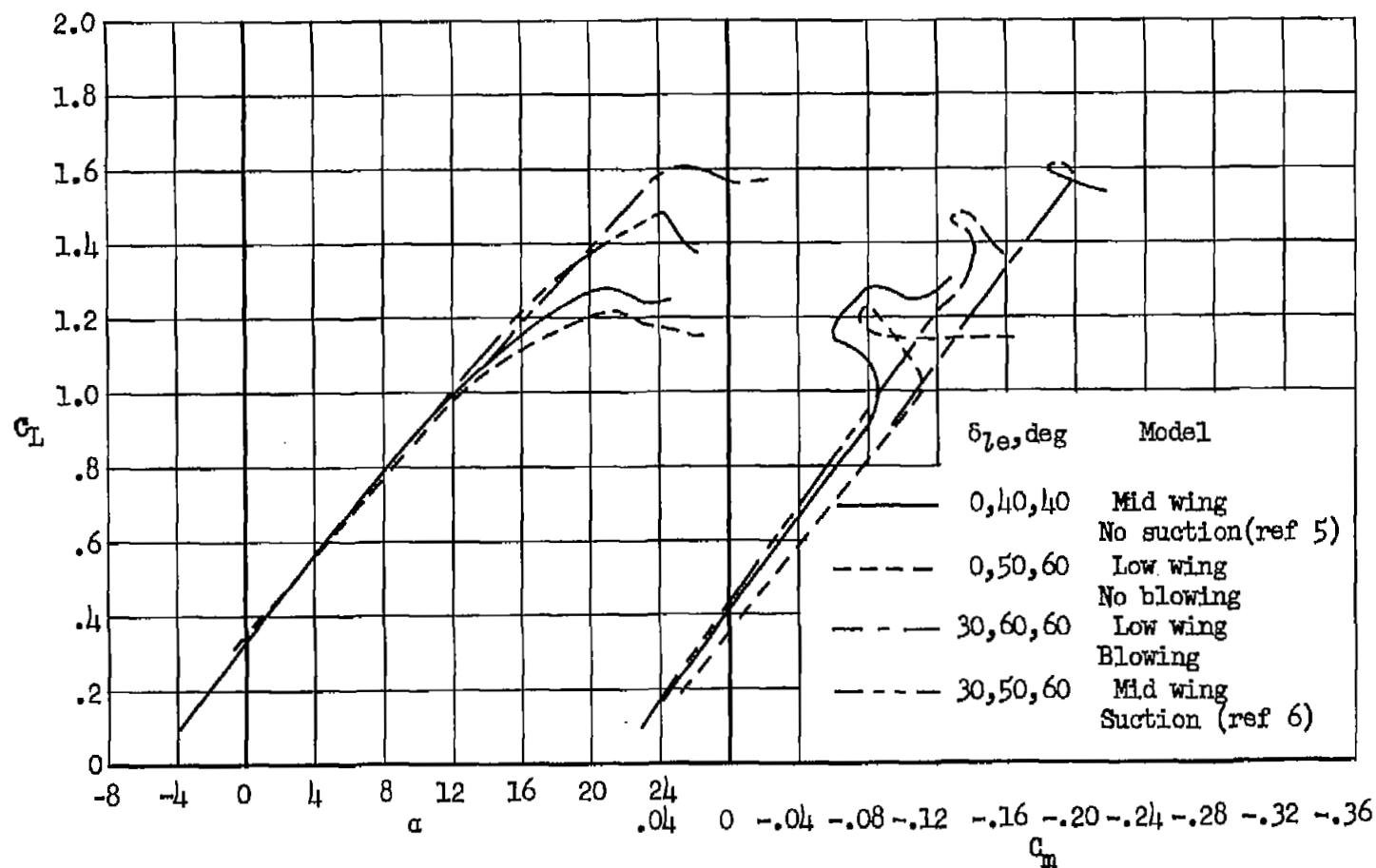
Figure 18.- Comparison of the longitudinal characteristics of the area suction model and the blowing model; leading edge BLC applied from $\eta = 0.4$ to 1.0; small-span trailing-edge flap, $\delta_{te} = 60^\circ$.
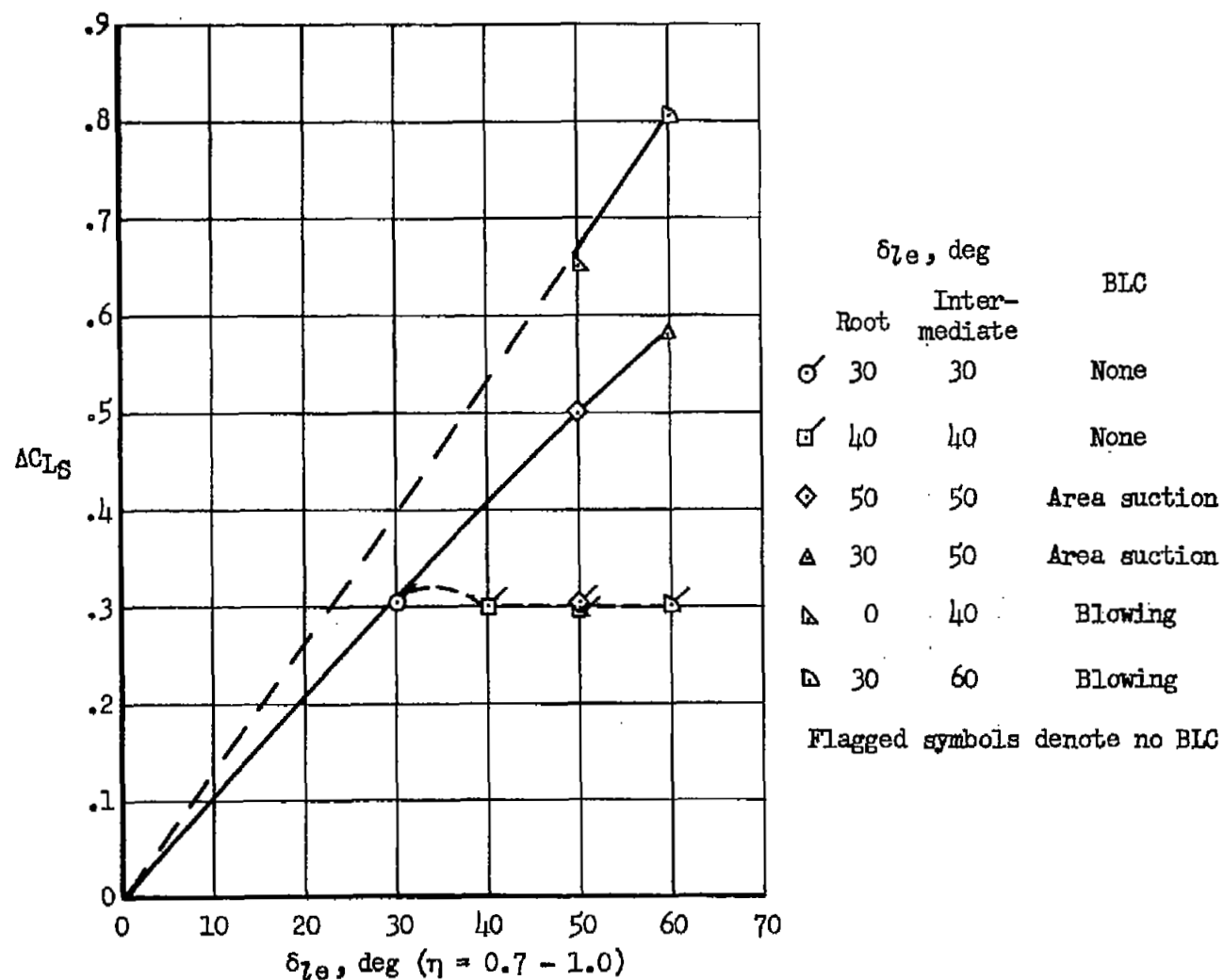
Figure 19.- The effect of outboard leading-edge flap deflection with and without blowing or area suction on delaying tip stall.
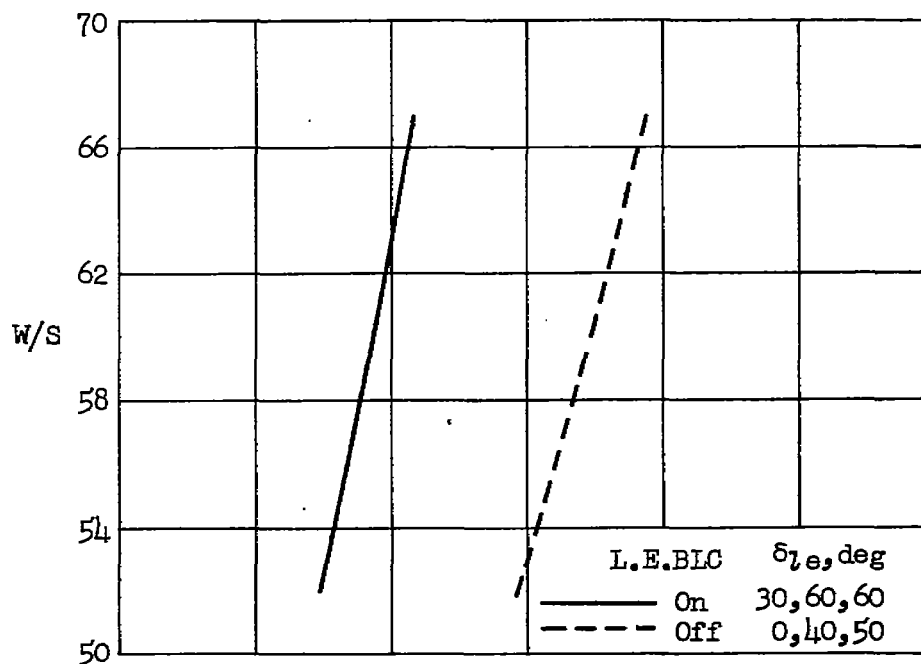
(a) Effect of leading-edge blowing BLC with small-span trailing-edge flap; $\delta_{te} = 60^\circ$, $C_{\mu te} = 0.006$.
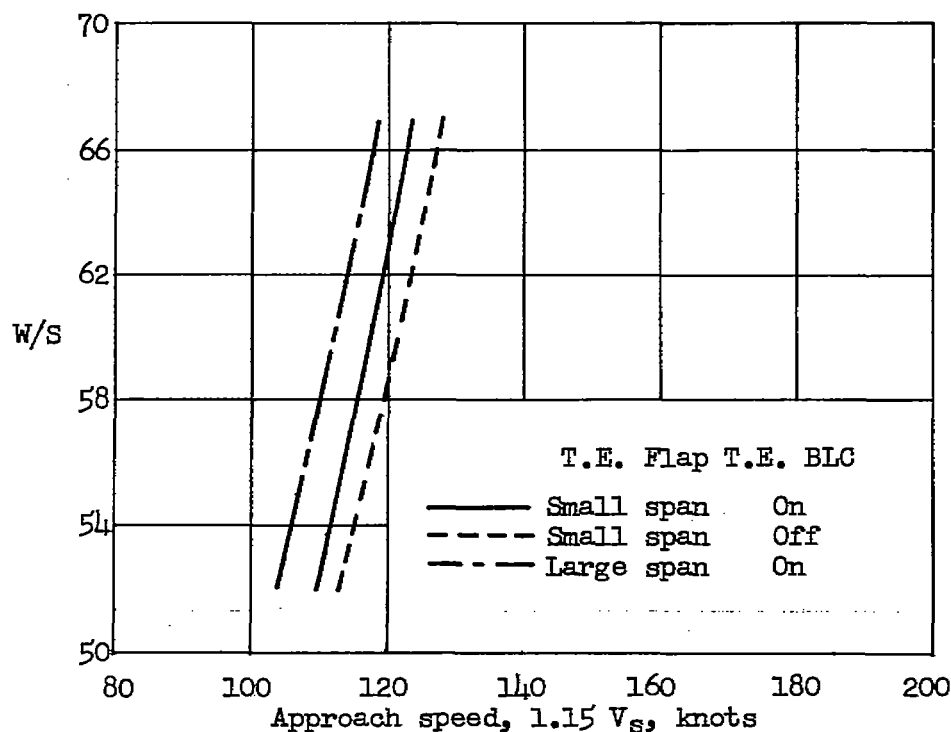
(b) Effect of trailing-edge flap span; $\delta_{te} = 60^\circ$ with leading-edge blowing BLC, $\delta_{le} = 30,60,60$.

Figure 20.- Effect of leading-edge and trailing-edge flap variables on approach speed with zero sinking speed.
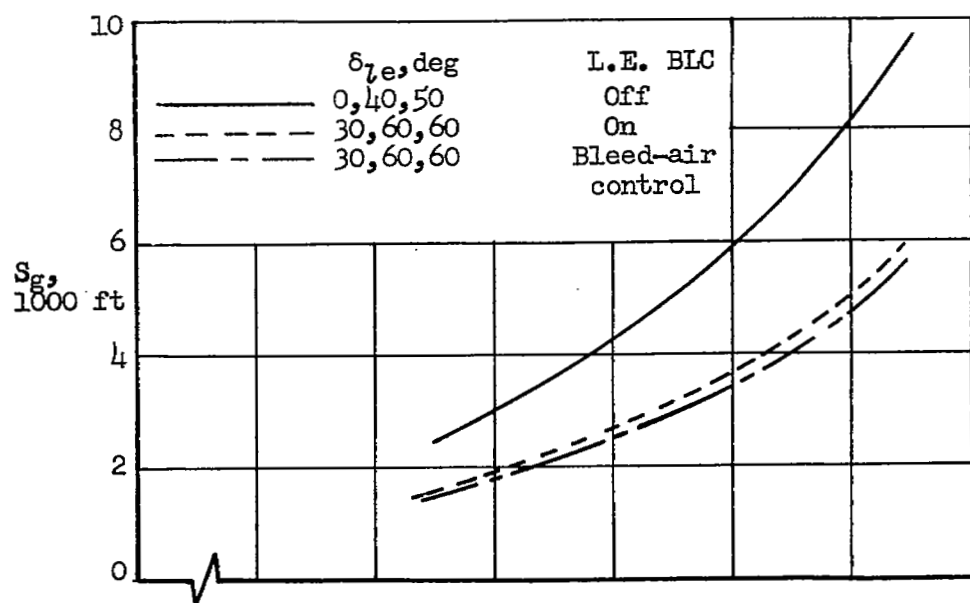
(a) Based on 1.05 V_S.
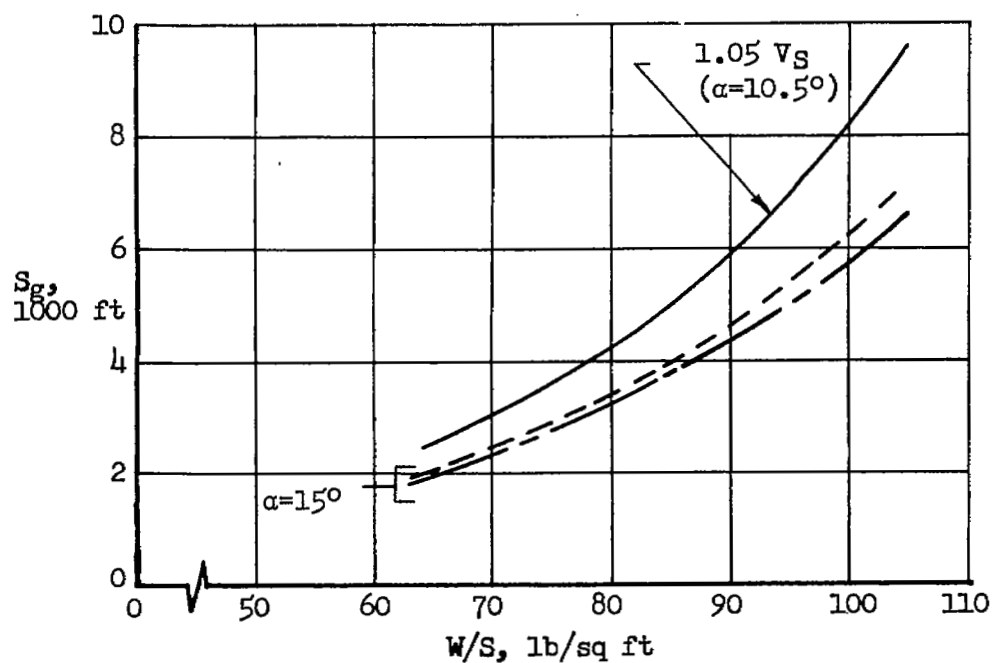
(b) Based on α limitation.

Figure 21.- Variation of take-off ground roll with wing loading; small-span trailing-edge flap with blowing BLC, $\delta_{te} = 60°$.
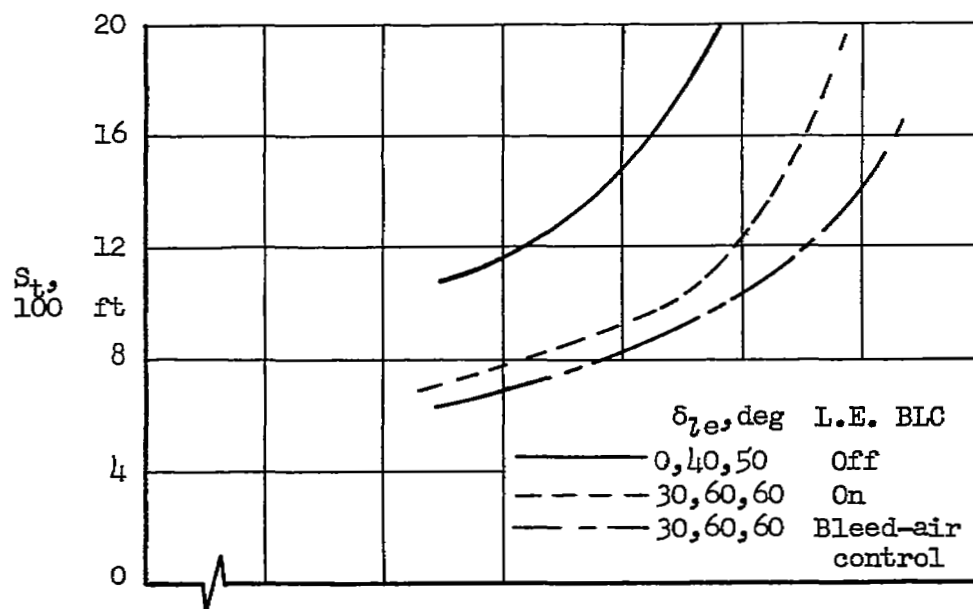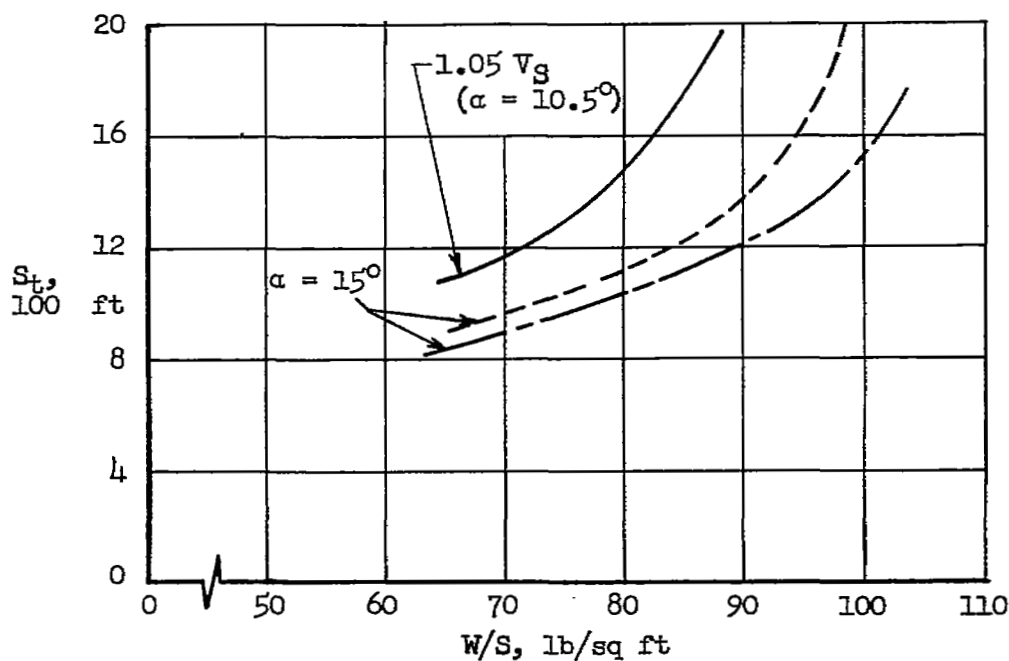
(a) Based on 1.05 V_S.

(b) Based on α limitation.

Figure 22.- Effect of leading-edge BLC on take-off air distance over a
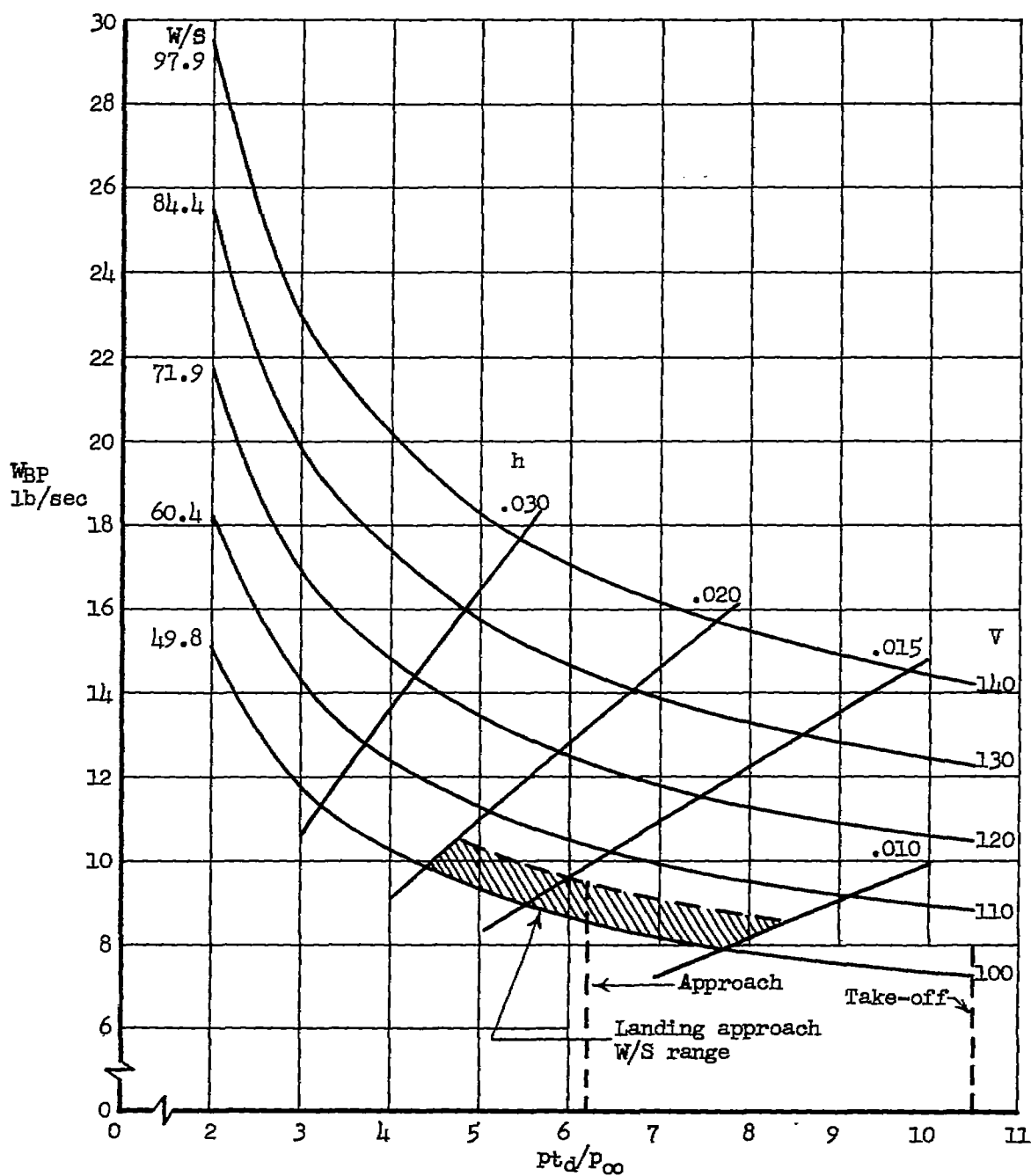50-foot obstacle; small-span trailing-edge flap with blowing BLC,
$\delta_{te} = 60^\circ$.
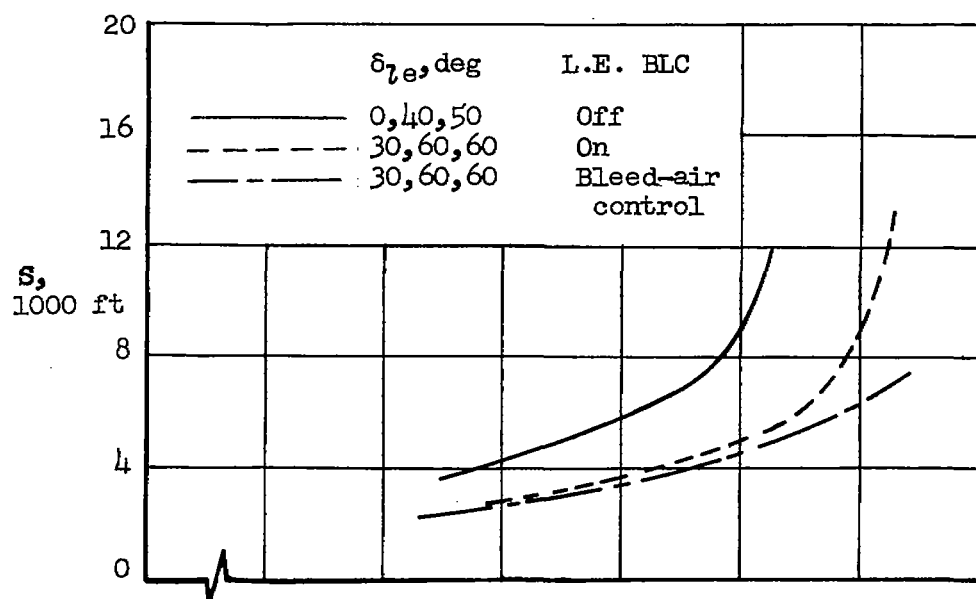
(a) Based on 1.05 V_S.
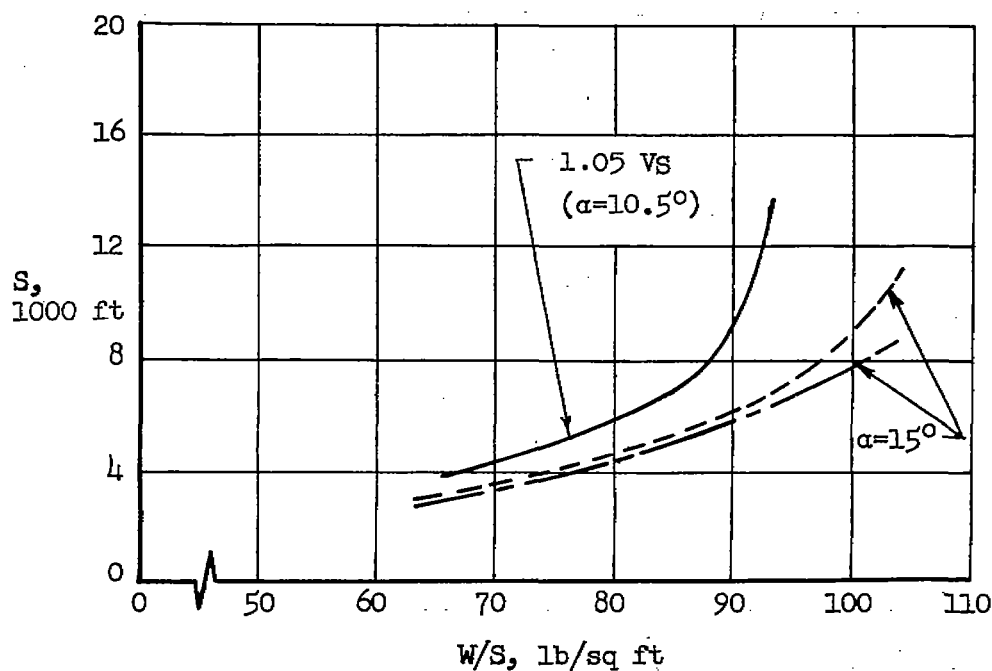
(b) Based on α limitation.

Figure 23.- Effect of leading-edge BLC on total take-off air distance over a 50-foot obstacle; small-span trailing-edge flap with blowing BLC, $\delta_{te} = 60^\circ$.

Figure 24.- Leading-edge nozzle height selection chart; δ_{le} = 30,60,60, $C_{\mu_{le}}$ = 0.032, trimmed C_L = 1.47, small-span trailing-edge flap deflected 60°.
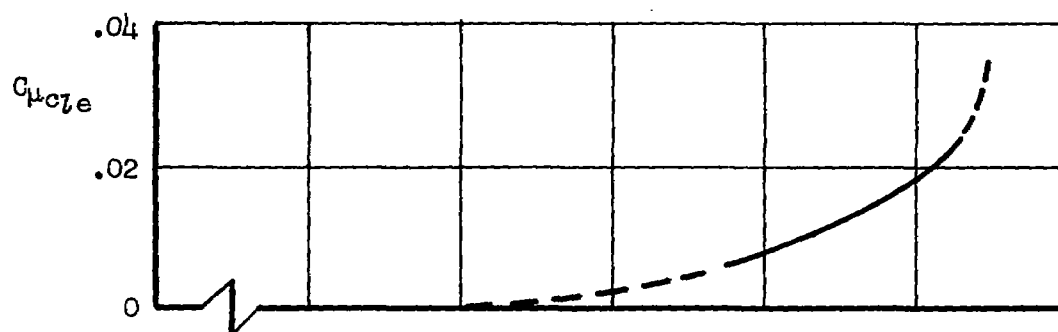
(a) Variation of $C_{\mu_{le}}$ required with α; leading-edge nozzle B.
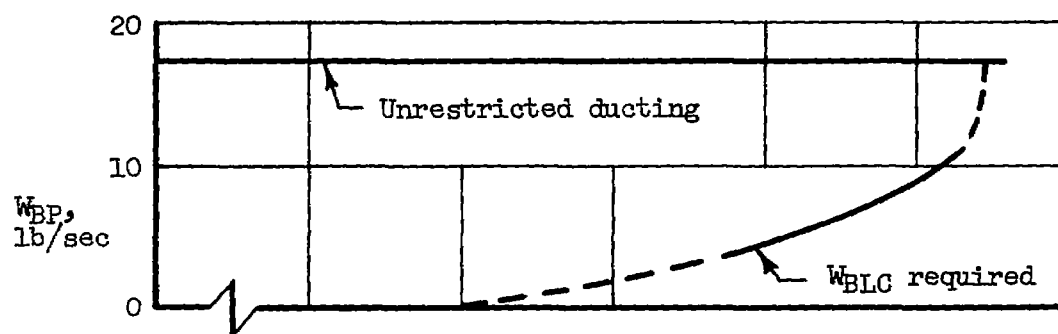
(b) Leading-edge air bleed flow required at 140 knots; h = 0.015.
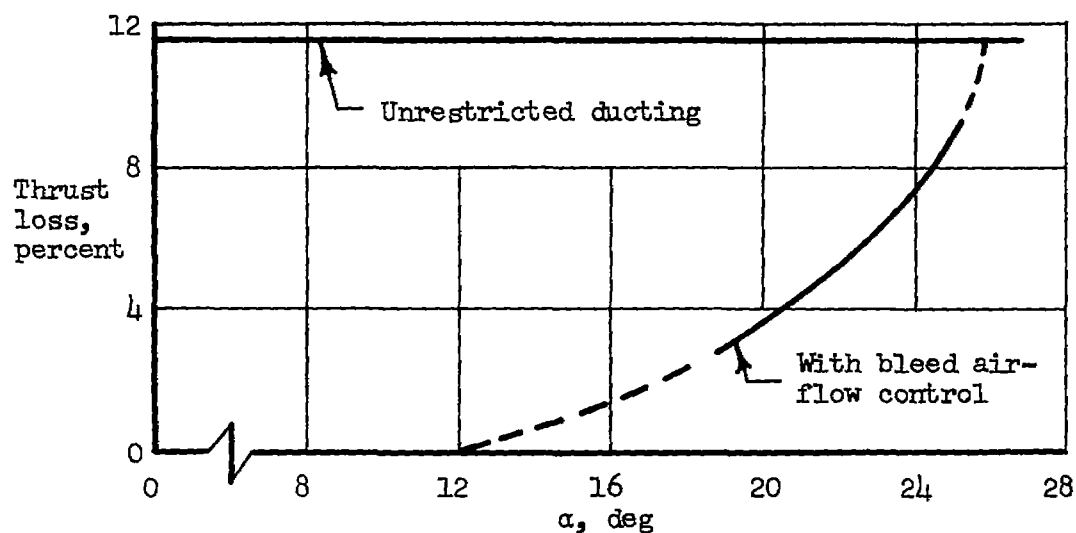
(c) Thrust loss caused by bleed air.

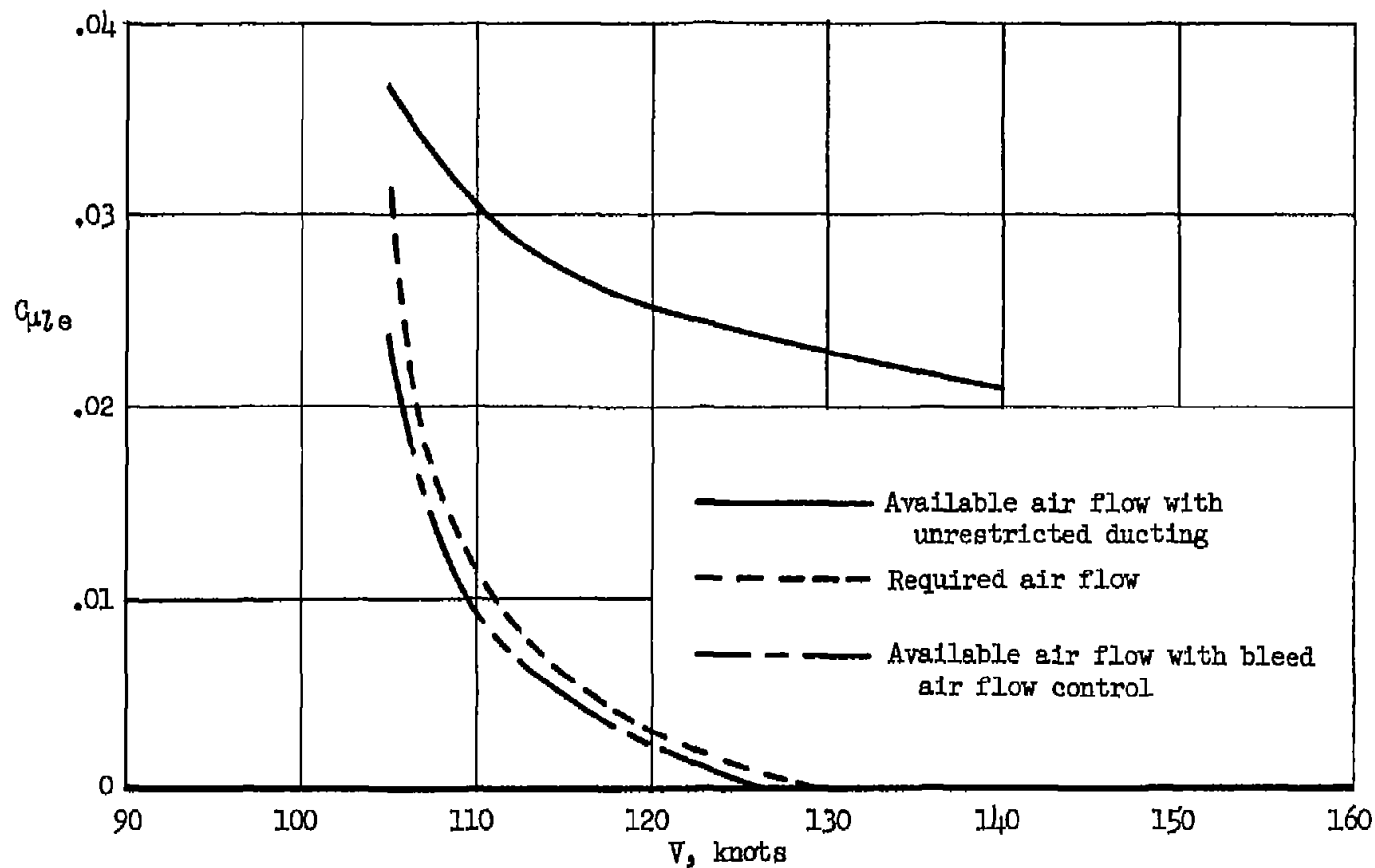Figure 25.- Engine bleed requirements and thrust loss due to unrestricted bleed at take-off.

Figure 26.- Effect on $C_{\mu l e}$ available with the bleed air-flow control in the leading-edge ducting; 10 ft/sec sinking speed, h = 0.015, W/S = 55 psf.